Hydrothermal sediment alteration at a seafloor vent field: Grimsey Graben, Tjörnes Fracture Zone, north of Iceland

Vesselin Dekov,[1] Jan Scholten,[2] Carl-Dieter Garbe-Schönberg,[3] Reiner Botz,[3] Javier Cuadros,[4] Mark Schmidt,[5] and Peter Stoffers[3]

Received 26 November 2007; revised 28 July 2008; accepted 21 August 2008; published 7 November 2008.

[1] An active seafloor hydrothermal system subjects the background sediments of the Grimsey Graben (Tjörnes Fracture Zone) to alteration that produces dissolution of the primary volcaniclastic matrix and replacement/precipitation of sulfides, sulfates, oxides, oxyhydroxides, carbonates and phyllosilicates. Three types of hydrothermal alteration of the sediment are defined on the basis of the dominant hydrothermal phyllosilicate formed: smectite, kaolinite, chlorite. The most common alteration is near-total conversion of the volcaniclastic material to smectite (95–116°C). The dominant smectite in the deepest sediments sampled is beidellite, which is replaced by montmorillonite and an intimate mixture of di- and tri-octahedral smectite up core. This gradual vertical change in smectite composition suggests an increase in the Mg supply upward, the result of sediment alteration by the ascending hydrothermal fluids mixing with descending seawater. The vertical sequence kaolinite → kaolinite-smectite mixed-layer → smectite from bottom to top of a core, as well as the distinct zonation across the veins (kaolinite in the central zone → kaolinite-smectite in the rim), suggests hydrothermal transformation of the initially formed smectite to kaolinite through kaolinite-smectite mixed-layer (150–160°C). The cause of this transformation might have been an evolution of the fluids toward a slightly acidic pH or a relative increase in the Al concentration. Minor amounts of chamosite fill thin veins in the deepest sections of some cores. The gradual change from background clinochlore to chamosite across the veins suggests that chamosite replaces clinochlore as Fe is made available from hydrothermal dissolution of detrital Fe-containing minerals. The internal textures, REE distribution patterns and the mode of occurrence of another magnesian phyllosilicate, kerolite, suggest that this mineral is the primary precipitate in the hydrothermal chimneys rather than an alteration product in the sediment. Kerolite precipitated after and grew on anhydrite in the chimneys. Oxygen isotope ratios are interpreted to reflect precipitation of kerolite at temperatures of 302° to 336°C. It accumulated in the hydrothermal mounds following the collapse of the chimneys and subsequent dissolution of anhydrite, thereby forming highly permeable aquifer layers underlying the vent field. Some kerolite was redeposited in the near vent field sediments by turbidity flows. The altered sediments are depleted in Mn, Rb and Sr, and enriched in U, Mo, Pb, Ba, As, Bi, Sb, Ag, Tl and Ga, as a result of leaching and precipitation, respectively. Conservative elements (Ti, Zr, Hf, Sc, Cr, Nb and Sn) are depleted or enriched in the altered sediments because of passive (precipitation or leaching of other phases) rather than active (because of their mobility) processes.

Citation: Dekov, V., J. Scholten, C.-D. Garbe-Schönberg, R. Botz, J. Cuadros, M. Schmidt, and P. Stoffers (2008), Hydrothermal sediment alteration at a seafloor vent field: Grimsey Graben, Tjörnes Fracture Zone, north of Iceland, *J. Geophys. Res.*, *113*, B11101, doi:10.1029/2007JB005526.

[1]Department of Geology and Paleontology, University of Sofia, Sofia, Bulgaria.
[2]International Atomic Energy Agency, Marine Environment Laboratories, Monaco, Monaco.
[3]Institute of Geosciences, University of Kiel, Kiel, Germany.
[4]Department of Mineralogy, Natural History Museum, London, UK.
[5]Leibniz-Institut für Meereswissenschaften, IFM-Geomar, Kiel, Germany.

0148-0227/08/2007JB005526$09.00

1. Introduction

[2] Hydrothermal circulation through the sediment blanket of a sedimented spreading center results in partial discharge of the hydrothermal fluid, change of its composition and extensive alteration of the primary sediment. This process has significant impact on seawater composition and on chemistry and physical properties of the crust [*Edmond*

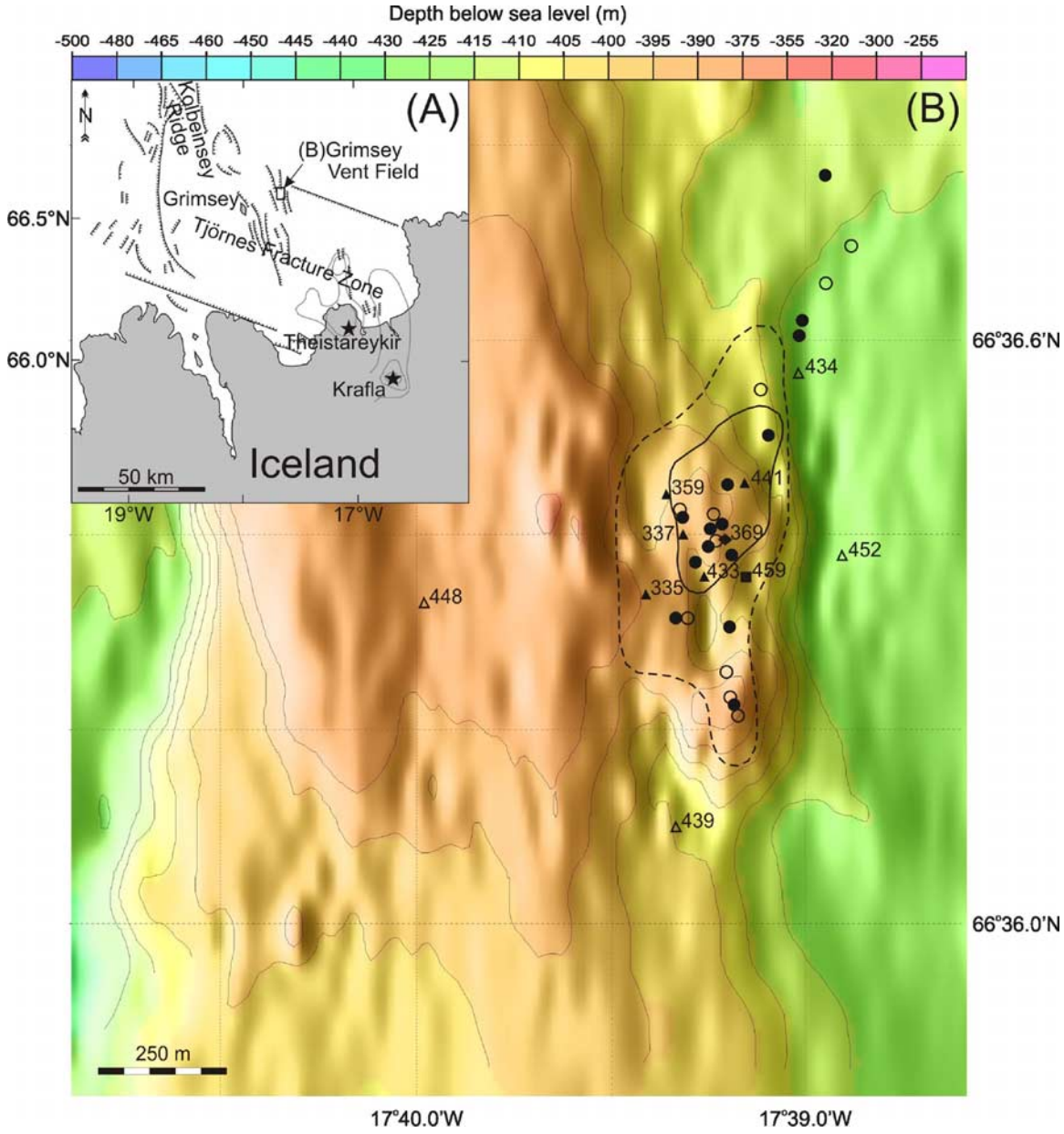

Figure 1. (A) Schematic map of the Tjörnes Fracture Zone north of Iceland (after *Rögnvaldsson et al.* [1998]). The Grimsey hydrothermal field is located at the eastern slope of a N–S striking ridge (box; mapped at Figure 1B). (B) Bathymetry of the Grimsey hydrothermal field (based on *Hannington et al.* [2001]) with location of the studied cores. Bold line, boundary of the central boiling zone; dashed line, extent of the bubble plume (in 1997); solid circles, boiling high-temperature vents; open circles, low-temperature (or not measured) vents; open triangles, background cores; solid triangles, cores with smectite alteration; solid diamond, core with kaolinite alteration [*Dekov et al.*, 2005]; solid square, core with kerolite layers; numbers next to the triangles, diamond and square, sampling site identification numbers.

et al., 1979] and therefore it is essential to be understood. Clay-dominated alteration of the sediment overlaying active spreading ridge has been used as an indicator of the types of physical-chemical processes taking place at three sediment-covered spreading centers: Guaymas Basin on the East Pacific Rise [*Lonsdale et al.*, 1980; *Koski et al.*, 1985], Middle Valley on Juan de Fuca Ridge [*Goodfellow and Blaise*, 1988; *Percival and Ames*, 1993] and Escanaba Trough on Gorda Ridge [*Zierenberg and Shanks*, 1994].

[3] Knowledge of hydrothermal alteration was notably absent for shallow-water sediment-covered spreading centers with boiling vent fluids. Such a new type of seafloor hydrothermal system was discovered in a sedimented rift east of Grimsey Island, north of Iceland (Figure 1) in 1997 and extensively studied (R/V *Poseidon* cruises, *Jago* submersible dives) in the subsequent years (POS-229 in 1997; POS-253 in 1999; and POS-291 in 2002) [*Hannington et al.*, 2001; *Riedel et al.*, 2001]. This contribution is intended

to develop the earlier studies by *Hannington et al.* [2001] and *Lackschewitz et al.* [2006] who reported on the sediment alteration at Grimsey field, but did not detail it. We aim at providing better insight into the hydrothermal alteration of the sediments at this distinctive new type of vent field and focus mainly on the hydrothermal phyllosilicates.

2. Geologic Setting

[4] The Grimsey vent field is situated east of Grimsey Island, ~30 km north of Iceland (Figure 1). It lies in the Grimsey Graben, a sediment-filled (buried to an average depth of 100 m; seismic data; T. Kuhn, personal communication, 2003) pull-apart basin within the Tjörnes Fracture Zone (TFZ) (Figures 1A and 1B). Glacial and volcaniclastic material supplied by both the ice-fed rivers draining the northern Iceland and volcanic eruptions fills the graben [*Hannington et al.*, 2001]. TFZ is a spreading axis offset, which links the north Iceland rift zone with the southern Kolbeinsey Ridge (Figure 1A) [*Rögnvaldsson et al.*, 1998]. It is a seismically active, 75-km-wide zone of dextral slip with oblique extension. The shallow-water (~400 m) vent field occurs near the summit of two mound structures on the eastern slope of a N–S striking ridge (Figure 1B) and is composed of about 20 anhydrite mounds (up to 10 m in diameter) and chimneys (1–3 m high) venting high-temperature (250°C), clear, metal-depleted hydrothermal fluids [*Hannington et al.*, 2001]. Two facets of the Grimsey hydrothermal fluid chemistry [*Lackschewitz et al.*, 2006] are essential for the current contribution: (1) Mg concentration in the fluids (37–44 mM) is supposed to reflect fluid-seawater mixing within the hydrothermal mounds; (2) SiO_2 concentration in the hydrothermal end-member (11 mM) presumably reflects extensive fluid-sediment reaction below the seafloor. Boiling hydrothermal springs and shimmering water (submersible observations), and hot sediments (up to at least 102°C; cored in the central part of the field) indicate that the entire vent field is thermally active and the fluid boiling occurs within the upflow zone beneath the hydrothermal mounds [*Hannington et al.*, 2001; *Kuhn et al.*, 2003]. A model of the possible hydrothermal circulation patterns at Grimsey vent field has been developed by *Kuhn et al.* [2003]. Around the vent field the seafloor has an undulating or hummocky surface inferred to be a sign of buried, old, dead hydrothermal mounds [*Hannington et al.*, 2001].

3. Material and Methods

[5] We investigated over 300 sediment samples [bulk, silt (2–63 μm) and clay (<2 μm) fraction] from 11 sediment cores (gravity corer; Table 1): 4 are situated within the central boiling zone; 3 outside it, but still in the hydrothermal field; and 4 outside the hydrothermal field as reference background sediment (Figure 1B). Sediment core temperatures (Table 1) were measured with a digital temperature probe inserted in the sediment at the ends of the core barrels on deck after recovery of the cores [*Hannington et al.*, 2001], and therefore record only minimum in situ temperatures and are limited by the boil point of seawater.

[6] All samples were freeze-dried, weighed and divided into a fine (<63 μm) and a coarse (>63 μm) fraction by wet sieving. Grain size separation into silt and clay fraction was performed by settling of water suspensions in standing cylinders according to Stokes' law [*Moore and Reynolds*, 1989]. Mineralogy of the bulk sediment, and silt and clay fractions was determined by X-ray diffractometry (XRD): Philips X-ray diffractometer PW 1710 with monochromatic Cu K_α radiation, 40 kV, 30 mA. X-ray scans of the bulk samples were performed from 2 to 70°2θ, with steps of 0.02°2θ, and velocity 1 s/step. Onboard smear-slides observations by conventional optical microscopy were combined with laboratory XRD studies to determine the relative proportions of the principal sediment-forming minerals (especially the X-ray amorphous volcanic glass). Oriented clay specimens were produced by vacuum filtration through a 0.15 μm acetate filter. Measurements were carried out on air-dried, glycol-saturated, and heated air-dried specimens (after heating at 400°C and 500°C). They were scanned from 2 to 40°2θ, with steps of 0.02°2θ, at 1 s/step. Randomly oriented specimens were produced to identify di- or tri-octahedral clay minerals from the 060 reflections (57–64°2θ scans, steps of 0.02°2θ, at 120 s/step). Chlorite and kaolin polytypes (for the kaolin minerals kaolinite vs. dickite) were determined by analysis of randomly oriented specimens: 33–47°2θ, 0.02°2θ steps, velocity 120 s/step; and 20–55°2θ, 0.02°2θ steps, velocity 60 s/step, respectively.

[7] The percentage of the swelling smectitic layers in the interstratified clay minerals was estimated by comparing our experimental patterns with the computer-modeled X-ray diffraction profiles by *Brindley and Brown* [1980].

[8] Scanning electron microscope (SEM) observations were made on Au-coated specimens of fragments of bulk samples and of selected (conventional stereo-microscope Olympus C3030-ADL) single mineral grains using a JEOL JSM-5410LV electron microscope.

[9] For major and trace element analysis, bulk sediment samples and separated clay-size (<2 μm) fractions were oven dried at 40°C and then ground. The major element composition was determined using a Philips (PW 1400) X-ray fluorescence (XRF) spectrometer and a JEOL JXA-8900R electron microprobe (V = 15 keV, I = 20 nA, electron beam diameter 3 μm). For XRF analysis, the samples were dried at 900°C and melted after mixing 600 mg of sample with 3600 mg of $Li_2B_4O_7$. For the microprobe analysis, the samples were prepared as polished sections and areas with voids were avoided. Trace elements were analyzed by ICP-

Table 1. Investigated Sediment Cores

Cruise No.	Site No.	Latitude (N)	Longitude (W)	Depth (m)	Temperature at Core Catcher (°C)
POS-253	335 SL	66°36.38′	17°39.47′	395	75
	337 SL	66°36.40′	17°39.34′	390	85
	359 SL	66°36.41′	17°39.42′	390	25.8
	369 SL	66°36.39′	17°39.23′	391	101.6
POS-291	433 SL	66°36.36′	17°39.24′	396	101
	434 SL	66°36.56′	17°39.01′	417	27.1
	439 SL	66°36.09′	17°39.36′	406	21.4
	441 SL	66°36.44′	17°39.27′	391	96
	448 SL	66°36.33′	17°39.98′	385	7.7
	452 SL	66°36.38′	17°38.88′	417	21.1
	459 SL	66°36.35′	17°39.18′	396	94.5

MS using a VG Plasma-Quad PQ 1. Total dissolution of the bulk sample was performed by pressurized HF-$HClO_4$-aqua regia attack [*Garbe-Schönberg*, 1993]. The accuracy of the analytical results was controlled by measuring international standard reference material: BHVO-1, BIR-1, MAG-1.

[10] Pore fluid samples were obtained from 2 sediment cores (434 SL, 441 SL) by high-purity (99.9990%) N_2 pressure filtration (all-Teflon pore fluid press) of sediment slices through 0.2 μm polycarbonate membrane filters. All sediment handling and sub-sampling was under high-purity N_2 sheeth gas using a plastic glove bag (AtmosBag TM) in order to avoid oxidation of reduced metal species. Extracted pore fluids were immediately acidified with subboiled nitric acid to pH < 2 and stored in sealed and cooled polypropylene microvials until analysis. Subsequent analysis of pore fluids was by ICP-MS (Mn, Li, U, Mo, Ba, Sb) and ICP-OES (Mg, Fe, Sr). Prior to the analysis the pore fluid samples were diluted 20-fold (ICP-MS) and 10-fold (ICP-OES) with 2% (v/v) subboiled nitric acid in the home lab. Indium, Re, and Y were used as internal standards, respectively. The calibration strategies were as in the study of *Garbe-Schönberg* [1993]. During the ICP-MS analysis a weak signal suppression originating from the seawater matrix was evident from the spiked seawater samples. This interference has been corrected. Certified reference materials NASS-5, CASS-4, NIST 1643d, and IAPSO were run as unknowns along with the pore fluid samples for validation of the calibration and as a concurrent check of accuracy.

[11] Prior to oxygen isotope analysis, clay samples were purified by differential density separation in several liquids and free Fe and Mn oxides were removed using the method of *Mehra and Jackson* [1960]. Six samples were found to be sufficiently pure (>95% monomineralic clays; XRD determination) for stable oxygen isotope measurements. Oxygen was extracted from silicates using the ClF_3 method [*Clayton and Mayeda*, 1963; *Borthwick and Harmon*, 1982]. The samples were transferred to Ni reaction vessels and dried for 2 hours at 150°C at high vacuum. They were then reacted with ClF_3 at 600°C for 12 hours. Oxygen was quantitatively converted to CO_2, which then was analyzed isotopically in a Finnigan MAT 251 stable isotope mass spectrometer. Oxygen isotope ratios are expressed in the conventional δ notation as deviation in per mil from standard mean ocean water (SMOW). The oxygen isotope value of the NBS-28 standard [*Matsuhisa*, 1974] was determined (n = 9) as $\delta^{18}O = 9.6 \pm 0.1‰$ VSMOW. The oxygen isotope values of the minerals were used to calculate mineral formation temperatures assuming water-mineral isotope equilibrium. Oxygen isotope equilibration temperatures were calculated using the fractionation equations of *Savin and Lee* [1988] for smectite (used for montmorillonite), of *Kulla and Anderson* [1978] for kaolinite (used for kaolinite-smectite), and P. J. Saccocia et al. (unpublished data, 2008; oxygen and hydrogen isotope fractionation in the serpentine-water and talc-water systems from 250° to 450°C: 1000 ln $\alpha_{talc\text{-}water} = 11.70 \times 10^6/T^2 - 25.49 \times 10^3/T + 12.48$) for talc (used for kerolite). Although *Lackschewitz et al.* [2006] have reported $\delta^{18}O$ values for the Grimsey pore fluids (−0.3‰) suggesting to consider them as vent fluid values, we calculated the mineral formation temperatures using both the pore fluid and seawater (0‰) $\delta^{18}O$ values. It is our notion that: (1) there is no a priori reason to consider that analyzed sediment pore fluids (even in hot, hydrothermally altered sediment) should have been representative for the hydrothermal fluids; (2) pure samples of Grimsey vent fluids cannot be obtained using Niskin bottles [e.g., *Lackschewitz et al.*, 2006].

4. Results

4.1. Background Sediments

[12] The Grimsey Graben sediments taken outside the hydrothermally active area (Figure 1B) can be considered to be background precursors of the altered sediments. The background sediments are composed mostly of volcaniclastic material. Volcanic glass, plagioclase (Na-anorthite, andesine), pyroxene (augite) and quartz (in descending order of their abundance) are the most abundant mineral phases in the background sediments and are present in both the coarse and clay sediment fractions. They are more abundant than clay minerals even in the <2 μm fraction. As no evidence for an *in situ* hydrothermal formation of quartz has been found (SEM observations) quartz is considered to be detrital in origin (presumably from rhyolitic and dacitic rocks in northern Iceland as well as ice-rafted by the East Icelandic Current from Greenland). The relatively fresh volcaniclastic material reveals some features of background seafloor weathering. Clays [montmorillonite, Al-illite and chlorite (clinochlore II b)], interpreted to be either product of this weathering or detrital, are sparse and show no trends in abundance or crystallinity with depth (on the basis of XRD studies).

4.2. Altered Sediments

[13] The cores from within the hydrothermal field have lithology that exhibits alteration features: dense network of veins and veinlets, and zones of gradual color and density changes. The hydrothermal circulation through the Grimsey sediments has resulted in dissolution of the parent volcaniclastic matrix, and replacement by/or precipitation of sulfides, sulphates, oxides, oxyhydroxides, carbonates and phyllosilicates. Primary (euhedral) and diagenetic (framboidal) pyrite and marcasite are the only sulfides found in the Grimsey sediments (Figures 2A and 2B). They appear as vein networks (euhedral), lenses (euhedral, framboidal) or single grains (framboidal) scattered in the sediment (XRD analyses, not shown). Marcasite occurs only in the deepest parts of the sediment cores, while pyrite was found throughout the cored sediment and in all sediment fractions. Anhydrite, gypsum and barite (Figures 2C to 2E) also occur in the deepest core sections. Jarosite (Figure 2F) is rare. Mn-siderite and Fe-rhodochrosite have been found in a few samples of one core only. Goethite is often observed in veins. Anatase occurs as traces in almost all the samples.

[14] Phyllosilicates are sensitive indicators of the physico-chemical conditions at seafloor hydrothermal sites and therefore they are a powerful probe to understand the hydrothermal processes. However, they have not been sufficiently investigated at these sites because sulfides, sulphates and oxyhydroxides have been given preference. On the basis of the dominant hydrothermal phyllosilicate at the Grimsey vent field, we identified 3 distinct types of hydrothermal alteration of the primary sediment, producing smectite, kaolinite and chlorite, respectively. We comment on them in the flowing sections.

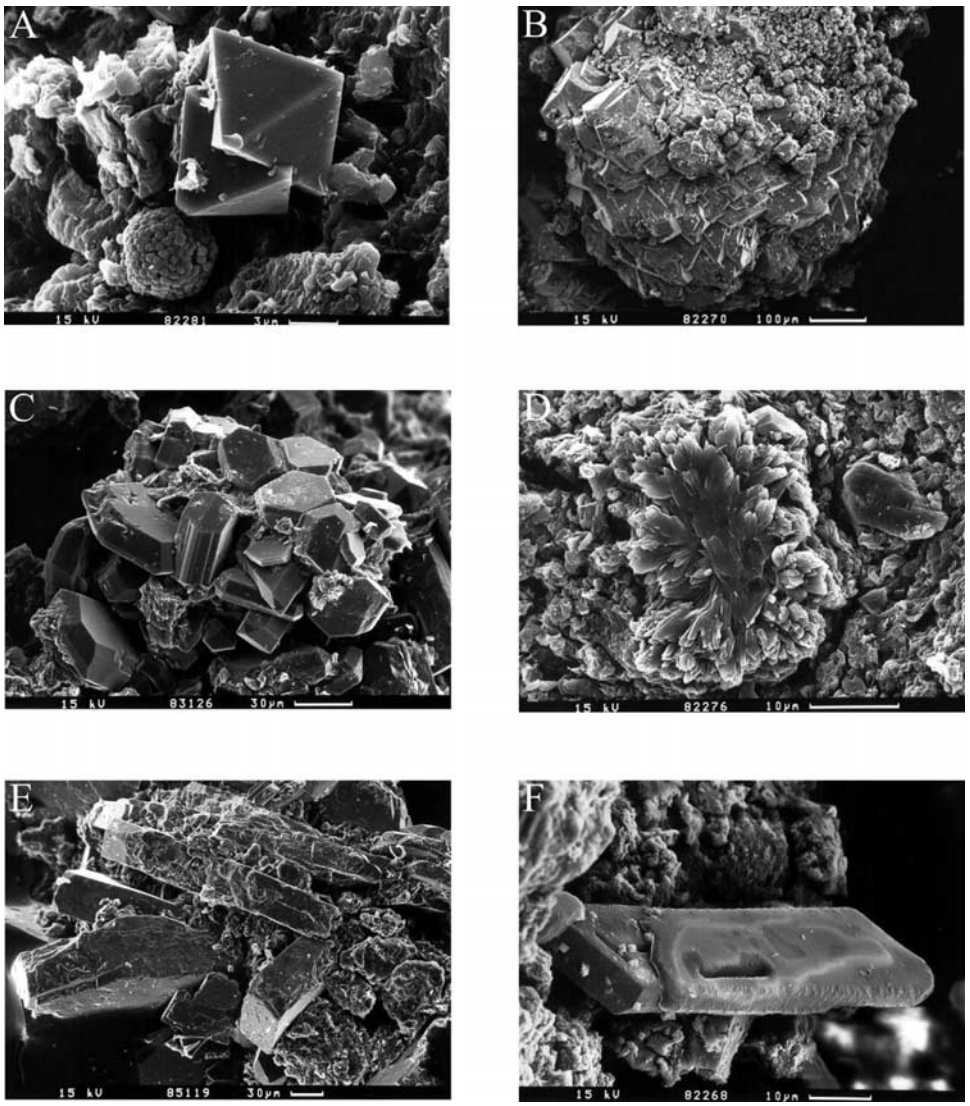

Figure 2. SEM micrographs (secondary electron images [SEI]) of altered sediments. (A) Euhedral (intergrowing octahedrons) and framboidal pyrite (sample 433 SL 352–356a). (B) Euhedral marcasite overgrown by a second generation of framboidal marcasite (sample 433 SL 352–356a). (C) Euhedral anhydrite (sample 369 SL 277–280). (D) Gypsum rosette in smectite matrix (sample 433 SL 352–356a). (E) Barite (sample 459 SL 184–188). (F) Jarosite crystal with dissolution and alteration features (sample 433 SL 352–356a).

4.2.1. Smectite Alteration

[15] Near-total conversion of the primary volcaniclastic material to smectite is the most common alteration of the Grimsey sediments. The matrix of six (335 SL, 337 SL, 359 SL, 433 SL, 441 SL, 459 SL) of the 11 studied cores consists of smectite. In the deepest horizons (>1.5 m) of the cored sediment, montmorillonite and beidellite (in almost equal proportions) are the only smectites (Figures 3 and 4A). Beidellite overgrows and replaces aluminosilicate grains forming a honeycomb texture (Figure 5A). It is almost purely aluminous smectite (Figure 5B). Montmorillonite forms tight stacks of flaky crystals (Figure 5C) and contains Mg and Fe (Figure 5D). The amount of beidellite decreases and montmorillonite dominates upcore (Figures 3 and 4A). From the middle core sections (~1.5 m) upward, the dominant smectite is an intimate mixture of di- and tri-octahedral smectite (Figure 3) with the 060 peak at 1.51–1.52 Å (an intermediate value between those of Fe-rich and Mg-rich smectite). Sediment alteration associated with veining is restricted to the vicinity of the veins. Montmorillonite is the main clay mineral in all zones across the veins, but the amount of beidellite gradually decreases from the vein halos to the veins (Figure 3).

4.2.2. Kaolinite Alteration

[16] Sediments at a site (369 SL) situated among several high-temperature vents in the Grimsey vent field (Figure 1B) were described in a previous study (Figure 3 in the study of *Dekov et al.* [2005]). These sediments exhibited features of severe hydrothermal alteration: near-total dissolution of the volcaniclastic material that composes the background sediment, sulfate and sulfide precipitation and kaolinitization. Smectite, precipitated in the shallowest sediment, is gradu-

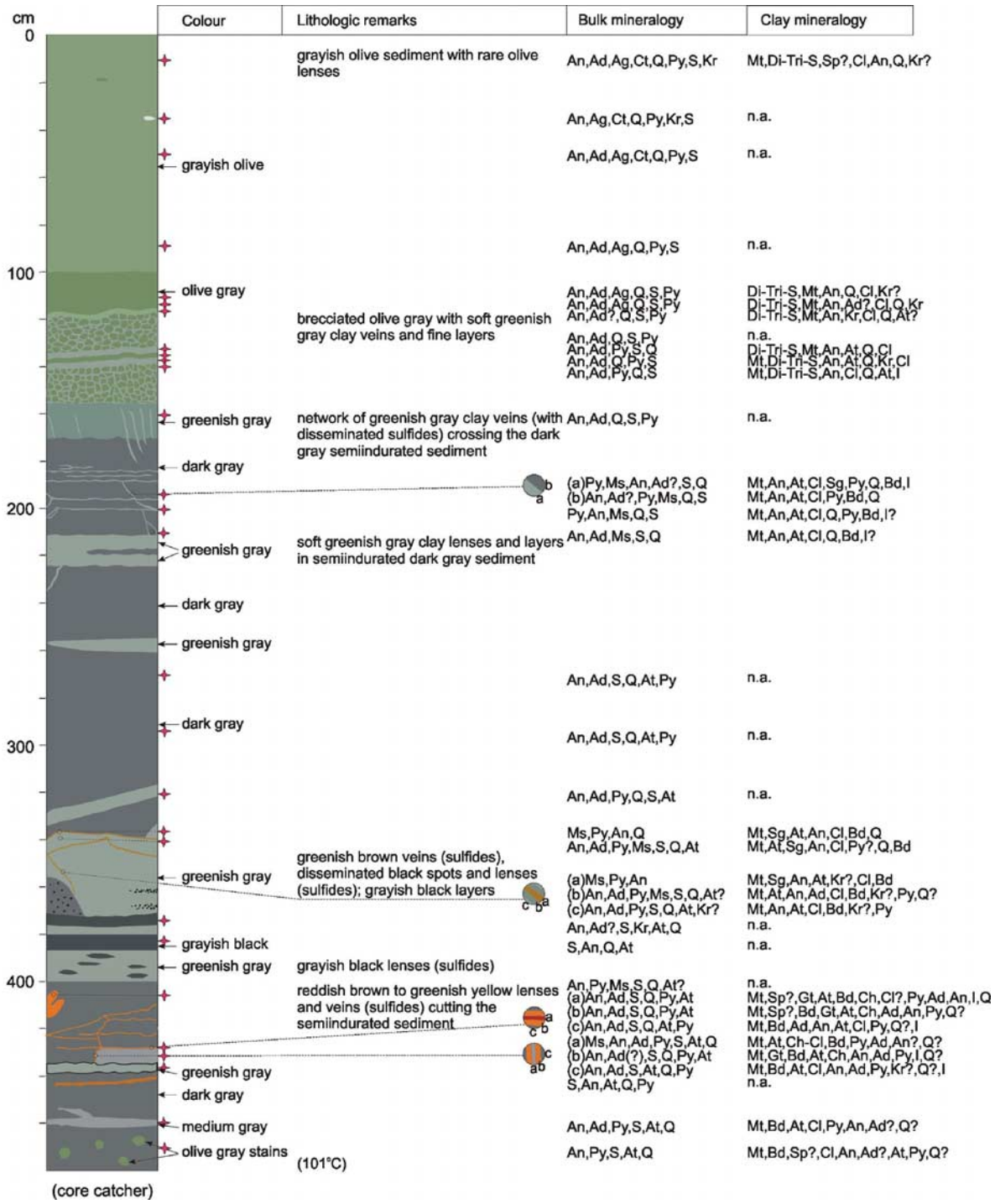

Figure 3. Schematic stratigraphic log of core 433 SL. Starlets, studied samples; n.a., not analyzed; Ad, andesine; Ag, augite; An, anorthite; At, anatase; Bd, beidellite; Bt, barite; Ch, chamosite; Cl, clinochlore; Cp, clinoptilolite; Ct, calcite; Gt, goethite; I, illite; Jr, jarosite; K, kaolinite; Kr, kerolite; Ms, marcasite; Mt, montmorillonite; Py, pyrite; Q, quartz; S, smectite; Sg, syngenite; Sp, saponite. These were arranged in descending order estimated according to the main peak intensities.

ally replaced downward by mixed-layer kaolinite-smectite and pure, well-crystallized kaolinite (Figures 4B, 4C, 5E, and 5F). No dickite was found. The extensive sulfate and sulfide precipitation in the lower section (>2 m) of the cored sediment and gradual kaolinitization of primary smectite down core (>0.8 m) is the essential difference between this and the other sites cored at Grimsey field.

4.2.3. Chlorite Alteration

[17] Trace amounts of magnesian chlorite (clinochlore) are present in almost all the samples. Detailed XRD studies showed this to be the monoclinic IIb-2 polytype. Since

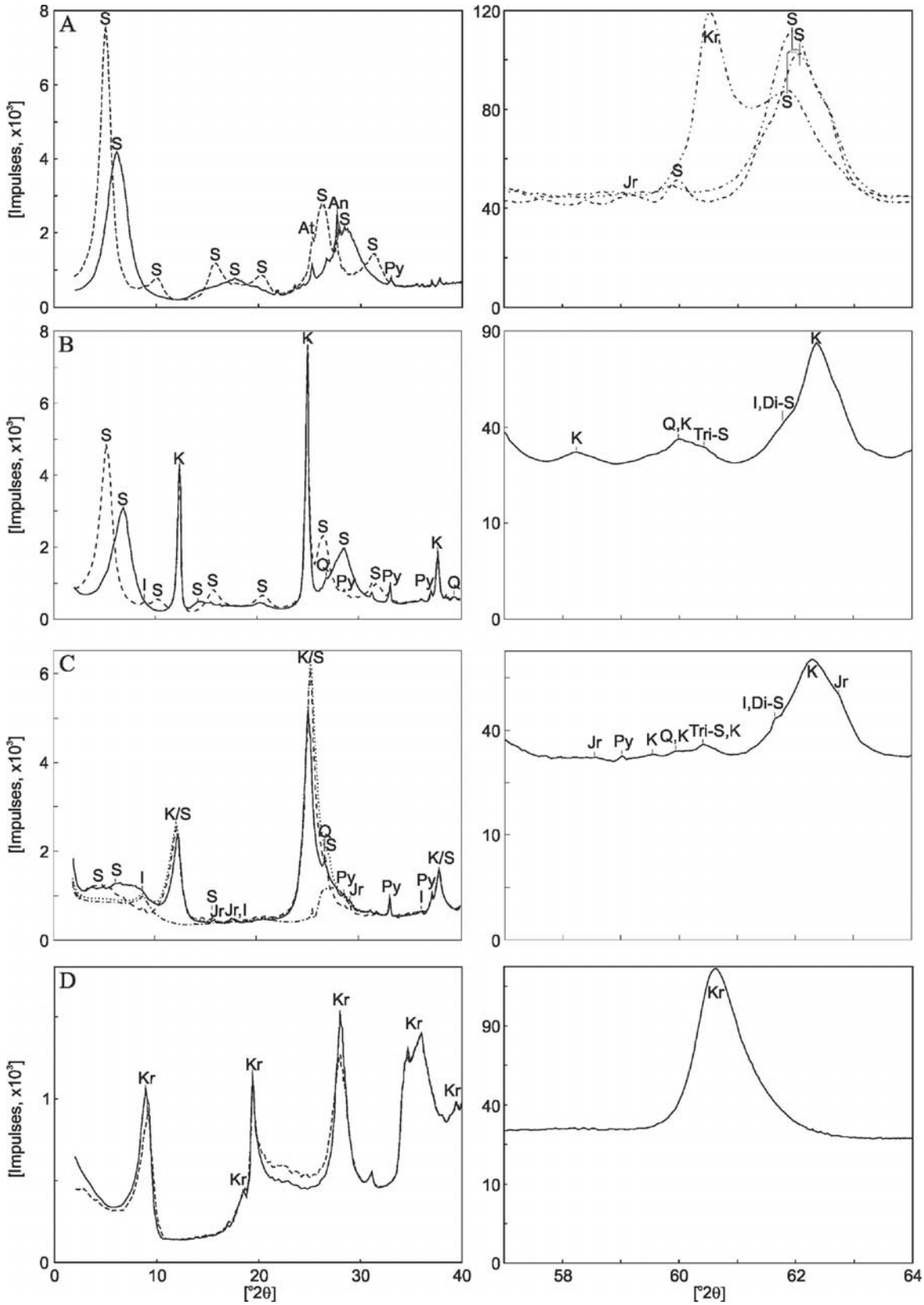

Figure 4

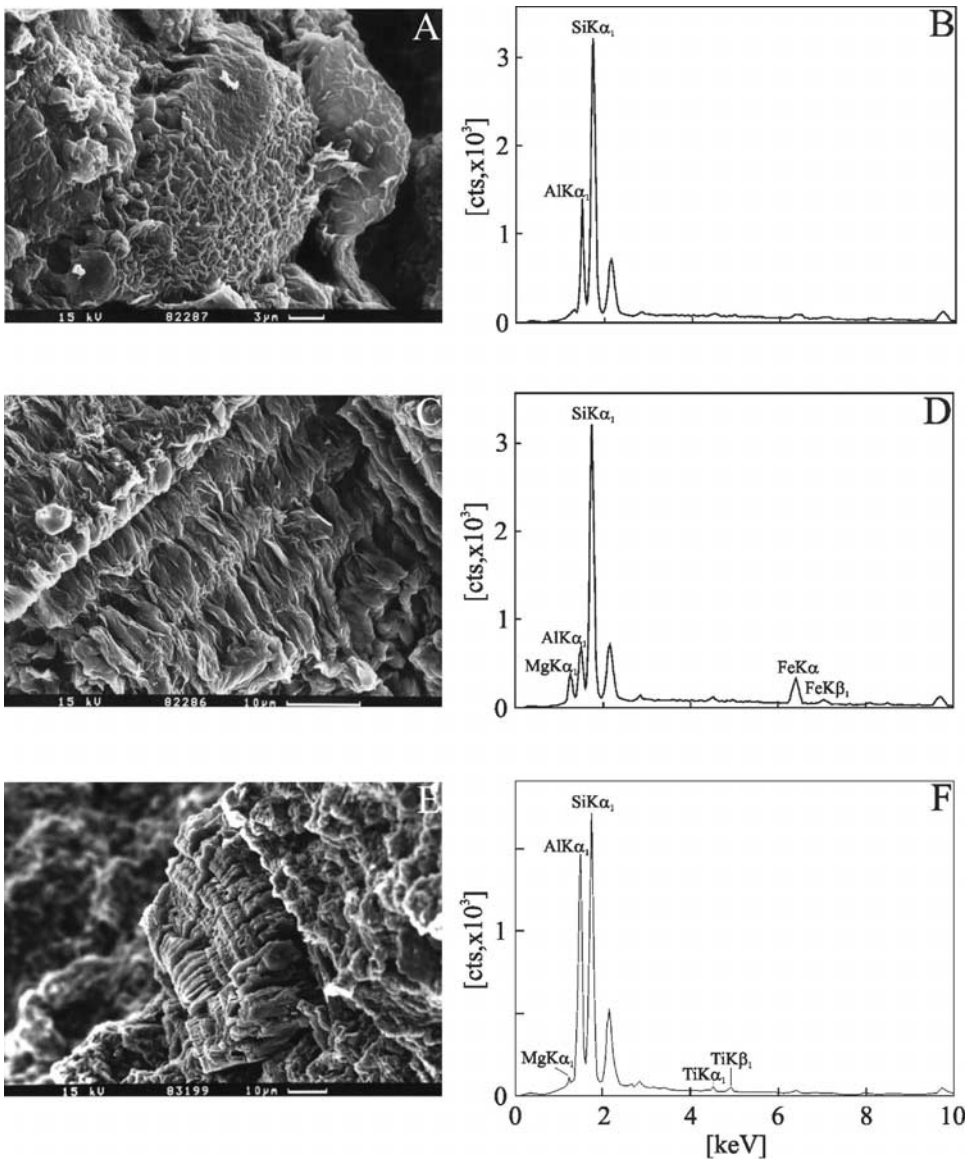

Figure 5. SEM micrographs (SEI) and EDS spectra of clay alteration products. (A) Honeycomb fabric of beidellite (sample 433 SL 404–406). (B) EDS spectrum of beidellite. (C) Stacks of flaky montmorillonite crystals (sample 433 SL 404–406). (D) EDS spectrum of montmorillonite. (E) Hexagonal kaolinite platelets forming a stack embedded in kaolinite and smectite matrix (sample 369 SL 253–255). (F) EDS spectrum of kaolinite. Unmarked peaks around 2 and 10 keV are those of Au from the coating.

traces of clinochlore are always present in the background Grimsey sediment as well, we consider that clinochlore is detrital (fluvial or ice-rafted from northern Iceland) rather than a hydrothermal alteration product.

[18] Minor amounts of ferrous chlorite [chamosite, orthohexagonal 1bb (β = 90°) polytype] fill thin veins in the deepest sections of some cores (Figure 3). The mineral association gradually changes across these veins (Figure 3): from major pyrite ± marcasite ± goethite in the vein through goethite + pyrite to pyrite traces in the background sediment, and chamosite ± clinochlore (vein) → chamosite → clinochlore (background sediment). In contrast to the ubiquitous smectite alteration and the local kaolinite alteration throughout the sediment at a site the chlorite alteration is

Figure 4. (left column) XRD patterns of oriented mounts and (right column) randomly oriented samples (analysis of the 060 peak). (A) Smectite (459 SL 225–226). (B) Sample with smectite and kaolinite (369 SL 267–269). (C) Sample with mixed-layer kaolinite/smectite (369 SL 80.5–83). (D) Kerolite (459 SL 155–158). For explanations, see Figure 3. Solid line, air-dried; dashed line, glycolated; dotted line, heated at 400°C; dot-dash line, heated at 500°C specimen; dot-double dash line, 459 SL 258–260; double dot-dash line, 459 SL 225–226; double dot-double dash line, 459 SL 184–188. Note the change of smectite (Figure 4A, right) from aluminous dioctahedral (beidellite) to magnesian-aluminous dioctahedral (montmorillonite) upward the core, i.e., the shift of the 060 peak toward lower angles.

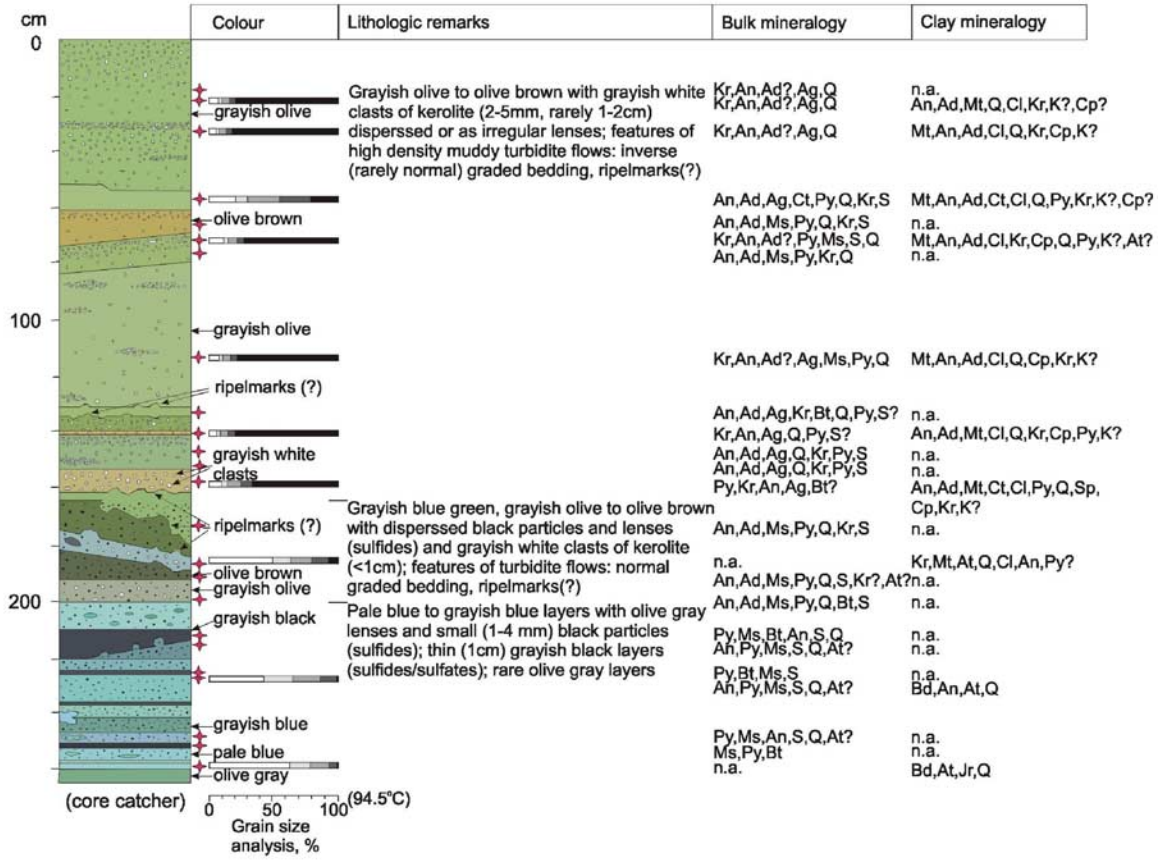

Figure 6. Schematic stratigraphic log of core 459 SL. Starlets, studied samples. For other explanations, see Figure 3. Grain-size analysis: white = <2 μm fraction; light gray = 2–6.3 μm; gray = 6.3–20 μm; dark gray = 20–63 μm; black = >63 μm.

minor and restricted within veins crossing the lower sections of the sediment altered to smectite.

4.2.4. Kerolite Precipitates

[19] The lithologic and grain-size studies showed that one of the cores (459 SL) exhibited inverse (rarely normal) graded bedding (clayey layer at the base, clayey with sand-sized particles in the middle, clayey with gravel-sized particles on top) and ripplemarks (Figure 6), which are typical features of high-density muddy turbidite flows. The coarse particles are relatively hard, angular to rounded (rarely), and 1–5 mm (rarely 1–2 cm) in size. These sediments were described on board as "ash layers" and are presumed to be hydrothermal aquifers at the Grimsey field, because of their relatively high permeability [*Hannington et al.*, 2001]. However, it appeared that all sand- and gravel-sized fragments from these layers were not ash, but kerolite lumps (Figure 4D) with the characteristic botryoidal habit of "talc" found lining the conduits of active chimneys [*Hannington et al.*, 2001; *Kuhn et al.*, 2003]. The perfectly rounded grains, originally thought to be ice-rafted debris, were kerolite as well. The kerolite lumps are crumbly, white, sometimes with a greenish or greyish hue on the surface, with a pearly lustre, and colloform with a mamillated surface (Figure 7A). The colloform bulbs are hollow, having cavities with square cross-sections (Figures 7A and 7H). We interpret the hollow prismatic cavities in the kerolite lumps to be casts of dissolved anhydrite crystals (see [40]). Small (~10 μm) botryoids of fine lamellar crystals (Figures 7C and 7E) grow on the internal layers of the kerolite lumps. The higher the Mg content in the botryoids (Figures 7B, 7D, and 7F) the better-crystallized are the kerolite crystals. Better-crystallized kerolite forms an open interlocking network (Figure 7G). The internal texture of the kerolite lumps is concentric (Figure 7H), with alternating fine layers of radiating kerolite. Tiny pyrite crystals occur scattered in the kerolite lumps (Figure 7H).

4.2.5. Sediment Geochemistry

[20] Major-element, minor-element and O isotopic composition of the smectite, kaolinite and kerolite are given in Tables 2 and 3. The variations in major-element composition of smectite (montmorillonite) and kerolite (Table 2) are in the theoretically expected frames for these mineral phases. The major-element composition of kaolinite-smectite varies noticeably (Table 2).

[21] The unusually high Ti content in montmorillonite and kaolinite (Table 2) is beyond the theoretically possible. This resulted in anomalous structural formulae for montmorillonite and kaolinite, if it is assumed that all of the Ti is incorporated in the clay minerals. We closely inspected the XRD patterns and came to conclusion that the elevated Ti concentrations were the result of analyzing fine anatase (TiO_2) particles along with the clays, either by the electron beam or by the bulk XRF analyses. We have therefore

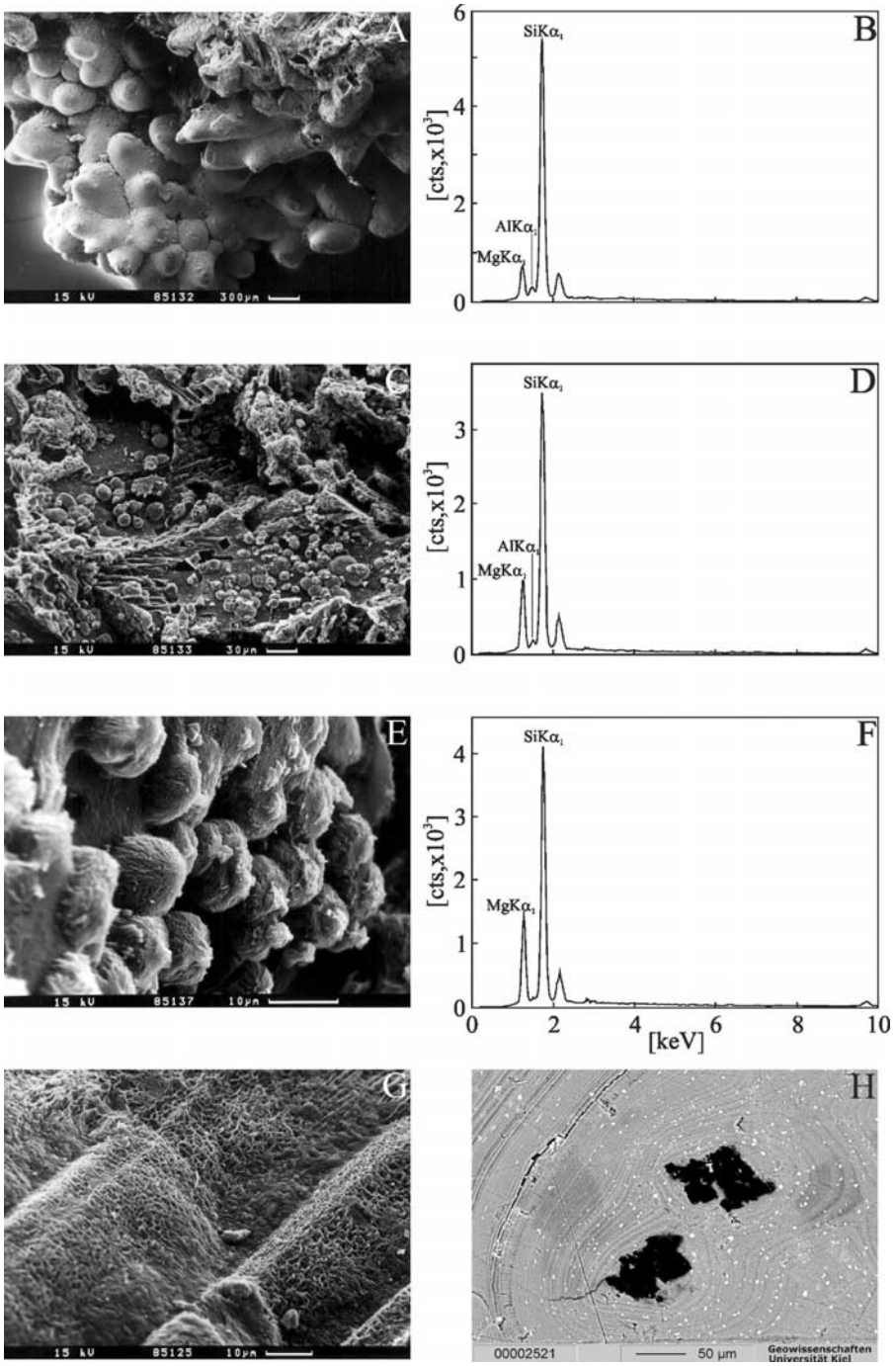

Figure 7. SEM micrographs and EDS spectra of kerolitic samples. (A) SEI of a greyish colloform lump, general view (sample 459 SL 155–158). Note the hollow casts with square cross-sections at the broken terminations of the colloform bulbs. (B) EDS spectrum of a colloform bulb (same specimen). (C) SEI of the inner part of a colloform lump (same specimen). Note the botryoids of fine lamellar crystals (kerolite, incipient crystallization), hollow casts of dissolved lath-shaped crystals and pyrite framboids. (D) EDS spectrum of a botryoid at stage of incipient crystallization (same specimen). (E) SEI of botryoids of fine lamellar kerolite crystals (same specimen). (F) EDS spectrum of kerolite (same specimen). (G) SEI of open interlocking, felted network of kerolite (sample 459 SL 155–158). (H) Backscattered electron image (BEI) of the polished section of a colloform lump (sample 459 SL 56–57). Note the alternating colloform growth of the radiating kerolite, the fine-grained sulfides (white particles) and the hollow casts at the center. Unmarked peaks around 2 and 10 keV (EDS spectra) are those of Au from the coating.

Table 2. Average Major-Element Composition (in wt. %), Structural Formulae, O Isotopic Composition and Calculated Temperatures of Formation of the Studied Clays (Representative Samples)

Sample No.	Clay	SiO_2	Al_2O_3	Fe_2O_3	TiO_2[c]	MgO	MnO	CaO	Na_2O	K_2O	P_2O_5	LOI	Total	Structural Formulae	$\delta^{18}O$ SMOW (‰)	T_1[d] (°C)	T_2[e] (°C)
459 SL 225–226[a]	Montmorillonite	51.6	17.5	4.22	3.02	7.2	0.01	0.28	0.31	0.3	0.15	24.3	108.9	$(Si_{3.77}Al_{0.23})_{IV}(Al_{1.28}Mg_{0.49}Fe^{III}_{0.23})_{VI}$ $(Mg_{0.30}Ca_{0.02}Na_{0.04}K_{0.03})_{int.}O_{10}(OH)_2$	12.9	116	112
459 SL 258–260[a]	Montmorillonite	49.7	18.8	5.82	3.00	5.44	0.01	0.08	0.18	0.59	0.14	24.4	108.2	$(Si_{3.69}Al_{0.31})_{IV}(Al_{1.34}Mg_{0.33}Fe^{III}_{0.33})_{VI}$ $(Mg_{0.27}Ca_{0.01}Na_{0.03}K_{0.06})_{int.}O_{10}(OH)_2$	14.6	98	95
369 SL 80–82.5[b]	Kaolinite-smectite	55.1	28.6	2.51	2.27	2.45		0.16	0.62	0.48			92.2				
369 SL 80–83.5[b]	Kaolinite-smectite	59.5	19.5	3.72	2.86	6.16		0.96	0.47	0.47			93.6				
369 SL 109–112[b]	Kaolinite-smectite	60.8	21.0	4.59	2.34	5.64		0.13	0.17	0.24			94.9		8.6	160	150
459 SL 31–32[b]	Kerolite	60.1	1.64	0.65	0.04	29.1	0.07	0.19	0.35	0.13			92.3	$(Si_{3.94}Al_{0.06})_{IV}(Mg_{2.84}Al_{0.06}Fe^{III}_{0.03})_{VI}$ $(Ca_{0.01}Na_{0.05}K_{0.01})_{int.}O_{10}(OH)_2$	2.0	336	330
459 SL 72–73[b]	Kerolite	59.1	1.27	0.40	0.02	29.0	0.09	0.25	0.23	0.08			90.4	$(Si_{3.94}Al_{0.06})_{IV}(Mg_{2.89}Al_{0.04}Fe^{III}_{0.02})_{VI}$ $(Ca_{0.02}Na_{0.03}K_{0.01})_{int.}O_{10}(OH)_2$	2.0	336	330
459 SL 155–158[b]	Kerolite	59.1	1.11	0.76	0.08	28.5	0.00	0.18	0.20	0.13			90.1	$(Si_{3.96}Al_{0.04})_{IV}(Mg_{2.85}Al_{0.05}Fe^{III}_{0.04})_{VI}$ $(Ca_{0.01}Na_{0.03}K_{0.01})_{int.}O_{10}(OH)_2$	3.3	308	302
459 SL 184–188[b]	Kerolite	59.6	0.81	0.34	0.01	28.6	0.03	0.06	0.14	0.07			89.7	$(Si_{4.00}Al_{0.00})_{IV}(Mg_{2.86}Al_{0.06}Fe^{III}_{0.02})_{VI}$ $(Ca_{0.00}Na_{0.02}K_{0.01})_{int.}O_{10}(OH)_2$			

[a]XRF data.
[b]Microprobe data.
[c]High concentrations for montmorillonite and kaolinite supposed to be due to presence of anatase.
[d]Calculated using $\delta^{18}O_{seawater} = 0‰$.
[e]Calculated using $\delta^{18}O_{Grimsey\ pore\ fluids} = -0.3‰$.

subtracted the Ti content when calculating the structural formulae of the montmorillonite and kaolinite. Structural formulae of montmorillonite (Table 2) were estimated on the basis of 22 oxygen atoms using the XRF data.

[22] The estimated structural formula of the kaolinitic material from the deepest horizon (core 369 SL), calculated on the basis of 18 oxygen atoms from the microprobe data (subtracting the Ti; see [21]) was:

$$(Al_{3.97}Fe_{0.03}Mg_{0.02})(Si_{3.94}Al_{0.06})O_{10}(OH)_8.$$

[23] This formula indicates kaolinite. The mixed-layer kaolinite-smectite contains up to 10% swelling smectitic layers (Figure 4C). Kaolinite-smectite is a hybrid between tetrahedral-octahedral-tetrahedral and tetrahedral-octahedral structures and the calculation of structural formulae is meaningless.

[24] The kerolite structural formulae (Table 2) were estimated on the basis of 22 oxygen atoms, using the electron microprobe data.

[25] The isotopic composition of the montmorillonite ($\delta^{18}O$ = 12.9–14.6‰) indicates temperatures of formation between 98° and 116°C if using $\delta^{18}O_{seawater}$, or 95–112°C when calculated with $\delta^{18}O_{Grimsey\ pore\ fluids}$ (Table 2). According to the oxygen isotope composition ($\delta^{18}O$ = 8.6‰), the kaolinite-smectite formed probably at T = 150°C (calculated with $\delta^{18}O_{Grimsey\ pore\ fluids}$) – 160°C (calculated with $\delta^{18}O_{seawater}$). The low $\delta^{18}O$ values (2.0–3.3) for kerolite suggest high temperatures of precipitation: 308–336°C (using $\delta^{18}O_{seawater}$), or 302–330°C (using $\delta^{18}O_{Grimsey\ pore\ fluids}$) (Table 2). The calculations for the montmorillonite and kaolinite-smectite temperatures of formation are more correct with $\delta^{18}O_{Grimsey\ pore\ fluids}$ since these clay minerals are sediment alteration products. As we do not have $\delta^{18}O_{vent\ fluid}$ data it would be equally correct to use either $\delta^{18}O_{seawater}$ or $\delta^{18}O_{Grimsey\ pore\ fluids}$ in the calculation of kerolite (vent precipitate) formation temperature. It can be seen that there is no substantial difference between either calculation and we have presented both sets of estimations (Table 2).

[26] The minor amount of chamosite vein filling did not allow us to separate enough material for detailed study.

[27] In respect to trace and rare earth element concentrations the unaltered background sediments exhibit a fairly narrow range of fluctuations (Table 3). Kerolite shows a pretty stable trace and REE composition, while the smectite and particularly the kaolinite display sizable trace and REE variations (Table 3).

4.3. Pore Fluid Chemistry

[28] The background sediment pore fluids have varying Mg concentrations (41.9–52.3 mM), but mainly less than that of the bottom seawater (51.2 mM [*Lackschewitz et al.*, 2006]) while the altered sediment pore fluids have Mg content (46.4–53.3 mM) about or exceeding that of the seawater (Table 4). Iron, Mn and Li concentrations of the background sediment pore fluids are less than those of the altered sediment pore fluids (Table 4). They show no clear trend down the background sediment core, while a substantial Fe, Mn and Li content increase is observed down the altered core (Table 4). Strontium is enriched in the altered sediment pore fluids relative to the background

Table 3. Trace and REEs in the Investigated Sediments (Representative Samples)

Sample No.	441 SL 185–190	441 SL 210–215	337 SL 239.5	369 SL 253–255	369 SL 267–269	459 SL 78–83	459 SL 106–111	434 SL 43–48	439 SL 45–50	448 SL 80–85	452 SL 45–50	BHVO-1	BHVO-1	BIR-1	BIR-1	MAG-1	MAG-1
Alteration	Smectite	Smectite	Smectite	Kaolinite	Kaolinite	Kerolite	Kerolite	Unaltered	Unaltered	Unaltered	Unaltered	Standard[a]	Standard[b]	Standard[a]	Standard[b]	Standard[a]	Standard[b]
Li, ppm	13.5	10.8	9.56	29.7	11.3	47.4	44.2	16.7	40.7	17.9	16.6	4.60	4.57	3.4	3.24	79	69.4
Sc	37.8	37.6	41.0	63.3	23.7	13.1	14.9	26.9	16.0	25.0	24.9	31.8	32.4	44	39.9	17.2	12.4
Ti	14,487	14,702	16,971	21,674	9522	6519	7080	11,134	7281	10,916	10,428	16,246	15,253	5755	5699	4502	4172
V	370	354	355	466	275	167	184	265	193	245	235	317	313	313	314	140	138
Cr	124	125	115	165	75	49.4	54.2	92.8	60.5	79.0	81.7	289	273	382	387	97	95
Mn	212	231	67.7	299	378	638	564	1094	776	1030	1021	1301	1300	1325	1313	759	747
Co	37.5	48.5	40.5	50.5	36.7	17.6	19.0	32.0	22.3	28.3	27.6	45	43	51.4	50.8	20.4	20.4
Ni	58.7	70.0	147	109	100	29.7	30.7	49.7	40.8	43.7	44.1	121	116	166	165	53	48.9
Cu	114	107	118	136	134	54.6	57.1	77.0	71.9	72.1	69.8	136	134	126	116	30	26.2
Zn	174	167	146	176	136	68.8	71.8	112	92.2	108	101	105	105	71	68.3	130	125
Ga	21.0	22.8	29.9	29.9	47.3	17.5	18.7	16.7	17.5	17.0	15.9	21	21.1	16	15.0	20.4	21.7
Rb	12.9	13.3	9.87	8.02	3.56	7.04	6.37	16.0	11.5	19.8	16.3	11	9.26	0.25	0.13	149	147
Sr	174	184	121	40	238	202	288	268	336	270	291	403	399	108	107	146	140
Y	38.8	37.6	39.5	29.9	10.5	15.2	16.7	29.4	20.3	31.8	29.0	27.6	25.3	16	15.1	28	23.8
Zr	160	168	174	216	101	71.0	77.2	138	94.1	150	141	179	165	15.5	13.9	126	93.8
Nb	19.4	20.4	21.3	25.8	11.5	8.69	9.58	17.2	12.8	19.9	17.3	17.1	17.2	0.55	0.51	12.0	14.1
Mo	7.49	1.69	24.7	45.5	77.3	1.20	1.82	1.50	1.08	1.77	1.73	1.02	0.98	0.6	0.1	1.60	1.03
Sn	1.82	1.93	2.27	2.31	1.12	0.81	0.88	1.55	1.16	1.88	1.63	2.10	1.97	0.65	0.74	3.60	3.55
Sb	1.82	0.85	1.09	1.55	5.59	0.65	0.54	0.56	0.83	0.61	0.56	0.16	0.17	0.58	0.52	0.96	0.96
Cs	0.65	0.64	0.35	0.41	0.21	0.30	0.30	0.69	0.46	0.79	0.69	0.13	0.11	0.005	0.004	8.60	9.04
Ba	325	676	2134	501	118	3992	5340	292	6417	185	189	139	138	7.00	7.15	479	490
La	18.1	17.6	19.4	17.8	4.6	7.51	8.14	15.2	10.9	18.7	15.8	15.8	15.2	0.62	0.56	43	40.4
Ce	38.4	39.0	42.9	44.3	13.8	16.8	18.3	33.4	23.9	40.5	34.6	39	37.8	1.95	1.96	88	83.1
Pr	5.61	5.72	6.24	6.66	2.17	2.45	2.65	4.85	3.40	5.73	4.97	5.7	5.64	0.38	0.39	9.30	9.86
Nd	24.5	25.1	27.4	29.0	9.75	10.7	11.6	21.0	14.6	24.0	21.1	25.2	24.9	2.5	2.48	38	38.2
Sm	6.24	6.41	6.92	7.27	2.43	2.77	3.02	5.19	3.69	5.87	5.28	6.2	6.12	1.1	1.10	7.5	7.29
Eu	2.13	2.19	2.41	2.14	0.76	0.96	1.05	1.72	1.21	1.82	1.70	2.06	2.22	0.54	0.56	1.55	1.52
Gd	6.98	7.02	7.63	7.02	2.33	3.08	3.32	5.66	4.00	6.18	5.66	6.4	6.41	1.85	1.83	5.8	5.91
Tb	1.17	1.17	1.26	1.17	0.39	0.50	0.54	0.95	0.65	1.03	0.94	0.96	0.98	0.36	0.37	0.96	0.94
Dy	7.23	7.28	7.78	7.08	2.32	3.06	3.34	5.76	3.98	6.26	5.76	5.2	5.53	2.5	2.71	5.2	5.11
Ho	1.44	1.43	1.54	1.34	0.45	0.61	0.66	1.14	0.78	1.23	1.13	0.99	1.01	0.57	0.59	1.02	0.96
Er	3.91	3.89	4.13	3.67	1.27	1.63	1.79	3.09	2.10	3.34	3.09	2.4	2.56	1.7	1.73	3.00	2.59
Tm	0.56	0.56	0.59	0.55	0.19	0.24	0.25	0.45	0.31	0.49	0.44	0.33	0.34	0.26	0.26	0.43	0.38
Yb	3.67	3.69	3.85	3.70	1.33	1.53	1.70	2.94	2.00	3.18	2.93	2.02	2.15	1.65	1.78	2.6	2.56
Lu	0.54	0.54	0.56	0.54	0.19	0.22	0.25	0.43	0.29	0.46	0.43	0.29	0.30	0.26	0.27	0.40	0.37

Table 3. (continued)

Sample No.	441 SL 185–190	441 SL 210–215	337 SL 239.5	369 SL 253–255	369 SL 267–269	459 SL 78–83	459 SL 106–111	434 SL 43–48	439 SL 45–50	448 SL 80–85	452 SL 45–50	BHVO-1	BHVO-1	BIR-1	BIR-1	MAG-1	MAG-1
Alteration	Smectite	Smectite	Smectite	Kaolinite	Kaolinite	Kerolite	Kerolite	Unaltered	Unaltered	Unaltered	Unaltered	Standard[a]	Standard[b]	Standard[a]	Standard[b]	Standard[a]	Standard[b]
ΣREE	120.5	121.7	132.5	132.3	42.0	52.1	56.6	101.8	71.9	118.7	104.0	-	-	-	-	-	-
(Ce/Ce*)[c]	0.93	0.95	0.95	0.99	1.06	0.96	0.96	0.95	0.95	0.95	0.95	-	-	-	-	-	-
(Eu/Eu*)[d]	0.98	0.99	1.01	0.89	1.03	1.00	1.01	0.97	0.96	0.90	0.94	-	-	-	-	-	-
La_N/Lu_N	3.60	3.50	3.73	3.53	2.59	3.60	3.54	3.81	3.97	4.36	3.97	-	-	-	-	-	-
Hf	4.72	4.91	5.21	6.47	2.89	2.08	2.33	4.03	2.73	4.49	4.13	4.38	4.74	0.6	0.63	3.7	3.21
Ta	1.18	1.24	1.34	1.61	0.71	0.54	0.60	1.05	0.77	1.22	1.14	1.10	1.10	0.04	0.04	1.10	1.01
W	0.43	0.33	0.57	1.03	0.52	0.12	0.11	0.32	0.22	0.41	0.36	0.27	0.23	0.07	0.02	1.40	1.52
Tl	0.45	0.16	0.25	2.14	8.68	0.10	0.21	0.09	0.18	0.10	0.09	0.06	0.04	0.01	0.00	0.59	0.69
Pb	4.97	4.14	6.00	6.01	1.42	6.30	2.77	3.60	3.10	3.99	4.02	2.08	2.18	3.00	3.16	24	29.4
Bi	0.05	0.05	0.04	0.06	0.03	0.02	0.02	0.04	0.03	0.05	0.04	0.02	0.01	0.02	0.01	0.34	0.39
Th	2.08	2.19	2.33	2.91	1.10	0.91	1.00	2.01	1.41	2.65	2.16	1.08	1.30	0.03	0.03	11.9	12.1
U	22.6	7.60	27.6	11.9	29.2	10.3	5.55	1.77	10.2	2.54	1.99	0.42	0.45	0.01	0.01	2.7	2.74

[a]Reference values.
[b]Values from this study.
[c]$Ce/Ce^* = 2Ce_N/(La_N + Pr_N)$.
[d]$Eu/Eu^* = 2Eu_N/(Sm_N + Gd_N)$.

sediment pore fluids ($[Sr]_{mean}$ = 76.8 μM in the altered core 441 SL; $[Sr]_{mean}$ = 57.1 μM in the background core 434 SL; Table 4). It shows upcore increase in the altered sediment and no vertical trend in the background sediment. The concentrations of U, Mo, Ba and Sb in the altered sediment pore fluids ($[U]_{mean}$ = 4.15 nM, $[Mo]_{mean}$ = 51.7 nM, $[Ba]_{mean}$ = 547 nM, $[Sb]_{mean}$ = 3.46 nM; core 441 SL) are lower than those in the background sediment pore fluids ($[U]_{mean}$ = 5.08 nM, $[Mo]_{mean}$ = 90.9 nM, $[Ba]_{mean}$ = 901 nM, $[Sb]_{mean}$ = 34.0 nM; core 434 SL) (Table 4).

5. Discussion

5.1. Sources of Background Sediment Material

[29] Interpretation of the origin of the background sediment requires knowledge of the geology of the surrounding formations. The closest possible provenance areas feeding the Grimsey Graben are the Kolbeinsey Ridge and north Iceland (Figure 1A). We therefore consider the Kolbeinsey basalts and the most common magmatic formations of north Iceland, Theistareykir basalts and Krafla rhyolites, to be possible contributors to the background sediments at the Grimsey Graben. We estimated the contributions of different possible sources using the REE distribution patterns. The REE distribution patterns of the Grimsey background sediments lie between those of the Krafla rhyolites and Theistareykir basalts and have similar features to them: enrichment in LREE relative to the HREE, no Ce anomaly (Figure 8A). The lack of Eu anomaly in the Grimsey background sediments could result from the counterpoise of the negative Eu anomaly of the Krafla rhyolites with the slightly positive Eu anomaly of the Theistareykir basalts (Figure 8A). Simple modeling (conservative mixing) suggests that a mixture of 40% average rhyolitic material from Krafla with 60% average basaltic material from Theistareykir explains the observed REE patterns of the Grimsey background sediment (Figure 8A). We acknowledge the minor discrepancies between the modeled mixture and background sediment and consider this tentative assessment our best estimation, which implies that the Krafla rhyolites and Theistareykir basalts are the sources of the volcaniclastic material forming the Grimsey background sediments. The mineralogical data ([12]) is also consistent with inputs from north Icelandic rhyolites and basalts. The southern Kolbeinsey Ridge basalts exhibit different REE patterns (depletion in LREE relative to the HREE) (Figure 8A) and their contribution to the Grimsey sediments is unlikely. The narrow stripe in which the Grimsey REE patterns plot suggests homogeneity of the background sediments throughout the studied area.

5.2. Hydrothermal Precipitates in Altered Sediments

[30] The presently venting Grimsey hydrothermal fluids do not contain enough metals and sulfur to precipitate abundant sulfides at the seafloor [*Hannington et al.*, 2001]. They display low Fe content (0.7 μM [*Lackschewitz et al.*, 2006]). The subseafloor boiling might have affected the metal-carrying capacity of the hydrothermal fluids and deposition of sulphides is assumed to occur at greater depth [*Hannington et al.*, 2001]. Therefore the source of Fe for pyrite and marcasite precipitation in the Grimsey altered sediments (upper 4.8 m of the sediment cover (the longest

Table 4. Pore Fluid Chemistry

Core No.	Horizon	Sediment Type	Mg mM	Fe μM	Mn	Sr	Li	U nM	Mo	Ba	Sb
434 SL	8–13	Background	50.7	3.66	3.74	79.1	19.6	3.6	43	429	16.3
	43–48		49.1	1.23	3.14	76.5	18.4	5.1	74	421	29.1
	147–152		43.9	8.54	2.10	62.0	15.5	2.9	94	638	27.2
	185–190		41.9	7.04	2.35	57.0	16.1	6.9	151	517	49.0
	205–210		43.5	3.98	1.84	60.0	15.8	3.0	90	536	32.0
	225–230		42.4	8.59	2.70	55.4	16.4	3.6	70	483	22.3
	245–250		50.7	0.97	2.07	66.0	18.3	1.5	47	654	13.5
	265–270		46.5	6.10	2.28	57.7	16.9	2.0	35	644	9.8
	285–290		44.3	9.81	2.11	56.0	16.6	11.3	180	683	59.5
	305–310		44.7	6.32	2.89	55.8	16.1	7.5	118	738	37.2
	325–330		43.1	3.37	2.34	52.7	15.6	7.0	109	741	40.6
	345–350		42.5	5.53	2.41	52.2	14.9	5.7	83	771	41.4
	365–370		46.6	7.59	2.32	55.2	16.5	7.4	101	920	56.0
	385–390		43.7	8.72	1.98	54.7	16.8	7.0	201	1000	60.8
	405–410		47.4	5.91	1.91	56.8	16.7	2.4	52	1069	13.0
	425–430		47.2	16.5	2.31	57.9	17.0	3.2	66	1200	26.3
	445–450		43.8	22.3	3.02	50.3	15.0	3.2	66	1183	29.7
	465–470		52.3	7.54	3.16	60.3	18.4	1.7	30	1496	19.3
	470–475		48.2	13.3	2.84	58.1	17.0	10.2	142	1468	29.6
	490–495		50.6	5.24	3.02	61.4	17.2	6.4	135	1552	55.1
	540–545		47.5	16.6	3.95	60.4	17.4	10.2	111	1932	65.5
	566–571		51.6	19.3	2.46	59.5	18.4	1.8	71	2102	30.8
441 SL	55–60	Altered	49.2	6.76	5.02	79.5	21.0	2.7	95	316	1.5
	85–90		53.3	34.9	7.06	85.3	22.4	1.9	50	502	0.9
	110–115		50.5	67.8	6.87	78.6	23.4	3.8	52	561	1.3
	155–160		51.0	140	11.6	74.5	26.9	7.0	44	654	3.5
	210–215		46.4	149	11.9	66.2	29.1	5.4	19	704	10.1

core studied)) is an important issue. A likely Fe source is the detrital Fe-containing minerals (e.g., volcanic glass, augite) abundant in the background sediment ([12]) which upon hydrothermal alteration would release large amount of Fe. Indeed, the pore fluid studies revealed (Table 4) that the Fe concentration in altered core pore fluids (mean 79.7 μM; core 441 SL) is about an order of magnitude higher than that in background core pore fluids (mean 9.47 μM; core 434 SL), two orders of magnitude higher than that in vent fluid (0.7 μM) and three orders of magnitude higher than that in bottom seawater (<0.05 μM). Thus we interpret the formation of Fe-sulfides in the altered sediments as a result of interaction of hydrothermal fluid and/or gas with seawater and detrital Fe-containing minerals. The occurrence of euhedral pyrite and marcasite in vein networks ([13]) suggests precipitation in the medium of circulating hydrothermal fluids (leaching Fe from the sediment), while the framboidal pyrite and marcasite scattered in the sediment or overgrowing primary sulfides filling veins are obviously diagenetic minerals precipitated from pore fluids. Goethite is probably a secondary mineral after pyrite and marcasite oxidation and its formation suggests changing conditions from reducing to oxidizing. A detailed investigation of sulfide and sulfate precipitation at the Grimsey vent field is expected to appear in light soon [Kuhn et al., unpublished data].

[31] Precipitation of authigenic Mn-siderite and Fe-rhodochrosite requires a high bicarbonate alkalinity, a very low S^{2-} concentration and high Fe^{2+} and Mn^{2+} concentrations in the pore fluid. We do not have data on the alkalinity and S^{2-} content of the Grimsey sediment pore fluids and can use as a first approach those of the vent fluids which show high alkalinity (2.4–3.0 meq/l) and very low S^{2-} ($[SO_4^{2-}]$ = 20.6–25.7 mM) content [*Hannington et al.*, 2001]. The concentrations of Fe^{2+} (see [30]) and Mn^{2+} (mean 8.47 μM in altered core (441 SL); mean 2.48 μM in background core (434 SL); 3.2 μM in vent fluid; <0.5 μM in bottom seawater) are fairly high in the pore fluids (Table 4). Hence, where the alkalinity is high and the S^{2-} concentration is low, Fe- and Mn-carbonate precipitation is possible in the pore space of sediment.

[32] Anatase is supposed to be an alteration product of Ti-magnetite from the volcanic glass (Ti-magnetite → Ti-maghemite → anatase). Its ubiquitous occurrence throughout the cored sediment suggests the process of anatase formation is another source (although minor; anatase is a trace mineral) of dissolved Fe released into the pore fluid.

[33] Overall, the precipitation of minor mineral phases like sulfides, sulphates, oxides, oxyhydroxides and carbonates in the Grimsey vent field sediment is spatially ubiquitous and appears to be essential feature of the hydrothermal alteration process.

5.3. Smectite, Kaolinite and Chlorite Alteration

[34] At the Grimsey vent field, hydrothermal smectite forms via alteration of sediment to Mg-Fe dioctahedral smectite. The occurrence of Mg-rich trioctahedral smectite (saponite) within the active vents [*Lackschewitz et al.*, 2006] is not proven in view of the incorrect interpretation of the XRD patterns (Figure 3 in the study of *Lackschewitz et al.* [2006]) and chemical data (Table 2 in the study of *Lackschewitz et al.* [2006]) for the investigated precipitates showing presence of kerolite-smectite mixed-layer, but not saponite. The analyses of submarine vent fluids [*Von Damm et al.*, 1985a, 1985b, 2005] as well as the experiments on basalt-seawater interaction [*Mottl and Holland*, 1978] show that the oceanic crust acts as a chemical sink for Mg and quantitatively removes it from circulating hot (70–500°C [*Mottl*, 1983]) hydrothermal fluids. Thus one of the key questions in respect to Mg-phyllosilicates precipitating at

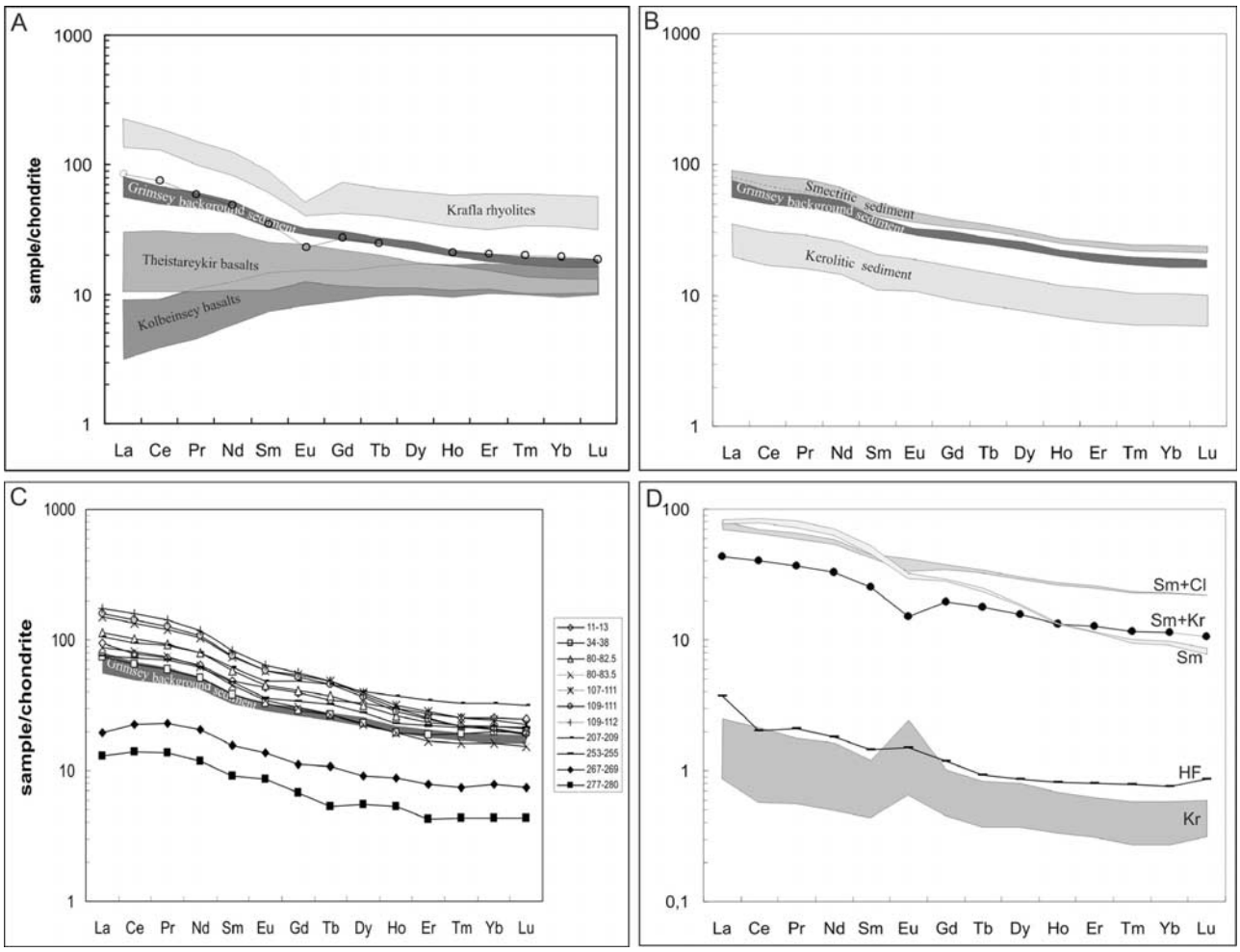

Figure 8. C1 chondrite-normalized [*Sun and McDonough*, 1989] REE distribution patterns for the following sediments, rocks and minerals. (A) Unaltered Grimsey background sediments (cores 434 SL, 439 SL, 448 SL, 452 SL), and three possible source areas: Krafla rhyolites [*Hemond et al.*, 1993], Theistareykir basalts (*Slater et al.* [1998]; Bondholshraun, Theistareykirhraun, and Asbyrgi flows from *Stracke et al.* [2003]), and South Kolbeinsey basalts [*Devey et al.*, 1994]; open circles, mixed model of 60% Theistareykir basalts and 40% Krafla rhyolites. (B) Altered smectitic (core 441 SL) and kerolitic (core 459 SL) sediments from the Central Boiling Zone. (C) Altered kaolinitic sediments (<2 μm fraction; core 369 SL) from the Central Boiling Zone. (D) Grimsey hydrothermal fluid (HF, sample 249-2, $\times 10^5$) and hydrothermal clays: kerolite (Kr, 459 SL 31–32, 459 SL 72–73, 459 SL 155–158), smectite (Sm, 459 SL 225–226, 459 SL 258–260), smectite + kerolite (Sm + Kr, 459 SL 184–188), smectite + chlorite (Sm + Cl, 337 SL 239.5, 433 SL 470–471).

this setting is the source of the Mg. Hydrothermal formation of Mg-phyllosilicates at mid-ocean ridge environment therefore requires either (1) entrainment or mixing of Mg-rich bottom seawater or Mg-rich pore fluids with the Mg-poor, silica-rich hydrothermal fluids at the vent site; or (2) redistribution of Mg (without leaching) during alteration of the sediment [e.g., *Saccocia and Gillis*, 1995]. Mg-metasomatism (1) has been suggested to occur at the other seafloor sediment-covered hydrothermal sites [*Koski et al.*, 1985; *Goodfellow and Blaise*, 1988; *Zierenberg and Shanks*, 1994], whereas Mg-phyllosilicate formation due to Mg redistribution (2) has been described in the shallow basement of the oceanic crust bellow active vent systems [*Saccocia and Gillis*, 1995].

[35] The vertical and cross-vein gradual change in smectite composition (from aluminous to magnesian upward and toward the vein center) suggests an increase in the Mg supply toward the seafloor and in the open cracks. This observation does not support an eventual scenario of Mg smectite formation through *in situ* Mg redistribution without leaching and removal [e.g., *Saccocia and Gillis*, 1995]. The presence of augite (Mg-containing aluminosilicate) in the upper horizons (<1.6 m) of some cores (Figures 3 and 6) and its absence in the lower horizons implies an additional Mg source to the upper part of the sediment. The upward increase in Mg in the cores could also be the result of hydrothermal dissolution of primary Mg-containing aluminosilicates (augite, volcanic glass) from the deeper sediments and upward transport of Mg leading to Mg-metasomatism of

the upper sediments. Indeed, the Mg content of the pore fluids ($[Mg]_{background\ sediment\ pore\ fluids} \leq [Mg]_{seawater}$; $[Mg]_{altered\ sediment\ pore\ fluids} \geq [Mg]_{seawater}$; Table 4) suggests an additional Mg source during sediment alteration. Definitely the Mg source to the upwelling hydrothermal fluids is not the downwelling seawater alone, but also the background sediment which upon hydrothermal leaching additionally supplies Mg to the system. The Mg smectite (montmorillonite and di-, tri-octahedral smectite) is therefore a result of sediment alteration by the ascending hydrothermal fluids (zero-Mg) mixing with descending seawater (Mg-rich) with the additional Mg supply from the background sediment. We suppose that the background sediment contributes to the net Mg balance of the alteration products at the other sedimented ridges as well via dissolution-reprecipitation mechanism.

[36] The noticeable major-, trace- and rare earth element variations in kaolinite-smectite (Tables 2 and 3) are supposed to be function of the percentage (5–10%) of the interstratifying smectitic layers. The vertical sequence kaolinite → kaolinite-smectite → smectite (core 369 SL; Figure 3 in the study of *Dekov et al.* [2005]) as well as the distinct zonation across the kaolinitic veins (almost pure kaolinite in the central zone and kaolinite-smectite along the rim) suggest hydrothermal transformation of initially formed smectite to kaolinite through mixed-layer kaolinite-smectite [*Dekov et al.*, 2005]. The d-spacing of the 060 peak (1.492–1.499 Å) seems to indicate that the original smectite was a montmorillonite with variable Mg content. Mg smectites form readily in alkaline and reducing environment [*Howard and Fisk*, 1988] more basic than that in the background seawater (pH > 8.5 [*Siffert*, 1962]). Mg smectite at site 369 SL is supposed to form [*Dekov et al.*, 2005] upon mixing of the hydrothermal fluids with seawater in a slightly alkaline and basic environment. Formation of kaolinite, on the other hand, occurs in neutral to slightly acidic conditions [*Huertas et al.*, 1999]. An evolution of the basic environment to slightly acidic might have been responsible for the transformation of smectite to kaolinite. Thus the initially formed smectite during the first basic stage has been subjected to transformation to kaolinite through interstratified kaolinite-smectite during the second neutral to acidic stage. Detailed kaolinitization scenario of the primary smectite at this site is given elsewhere [*Dekov et al.*, 2005].

[37] The gradual change in the mineral association across some veins [major pyrite ± marcasite ± goethite (vein) → goethite + pyrite → pyrite traces (background sediment), and chamosite ± clinochlore (vein) → chamosite → clinochlore (background sediment) (Figure 3)] suggests that chamosite is an alteration mineral. It probably replaces the primary detrital magnesian chlorite in microenvironments where Fe^{2+} is made available through hydrothermal dissolution of detrital Fe minerals ([30]) [e.g., *Komninou and Sverjensky*, 1995; *de Oliveira and Santos*, 2003].

[38] Previous studies on hydrothermal sediment alteration at sediment-covered spreading centers revealed that the most common phyllosilicates were Mg smectites. In the hydrothermally altered Middle Valley sediments, Mg smectite is gradually replaced by chlorite-smectite and Mg chlorite deep in the sediment [*Buatier et al.*, 1995; *Lackschewitz et al.*, 2000]. Similar vertical sequence has been established in the altered sediments of the Escanaba Trough [*Zierenberg and Shanks*, 1994]: Mg-Fe smectite in the top → Mg chlorite deep in the sediment. Smectite and chlorite are also the main phyllosilicates in the altered Guaymas Basin sediments [*Koski et al.*, 1985]. At the Escanaba Trough, *Zierenberg and Shanks* [1994] described an additional, third alteration type, talc alteration. *Koski et al.* [1985] also describe talc in the Guaymas sediments. Each of these three types of alteration is considered to involve addition of Mg from seawater, which penetrates down and mixes with ascending hydrothermal fluid and thus the alteration type depends on the depth in sediment [*Zierenberg and Shanks*, 1994; *Buatier et al.*, 1995; *Lackschewitz et al.*, 2000]. However, Mg input to the hydrothermal alteration process does not necessarily require seawater Mg source, but can also result from local redistribution of Mg originally present in the background matrix (sediment, rock) [e.g., *Saccocia and Gillis*, 1995]. Additionally the alteration type is a function of proximity to the heat source (i.e., thermal gradient). Although the hydrothermal setting at Grimsey Graben differs from that at the other sediment-covered spreading centers (background sediment subjected to alteration: volcaniclastic *vs.* hemipelagic terrigenous; hydrothermal fluids: boiling *vs.* non-boiling) the main alteration type is also Mg smectite. However, the evolution of the hydrothermal system from slightly basic to slightly acidic leads to gradual replacement of the primary alteration type, smectite, with kaolinite through kaolinite-smectite at Grimsey [*Dekov et al.*, 2005]. Chlorite alteration type is not magnesian (clinochlore), as at the other sedimented ridges, but ferrous (chamosite), which is interpreted to be a result of replacement of the detrital clinochlore where dissolved Fe^{2+} is sufficiently available. Kerolite, which is highly disordered talc, is not a sediment alteration type at Grimsey, but rather a chimney precipitate redeposited in the sediments after chimney collapse.

5.4. Kerolite Precipitation, Resedimentation and Aquifer Formation

[39] Previous studies report talc [*Hannington et al.*, 2001; *Lackschewitz et al.*, 2006] and mixed-layer kerolite-stevensite [*Kuhn et al.*, 2003] lining the conduits of the Grimsey vents. In the Grimsey sediments, we found kerolite (Figure 4D) and kerolite-smectite mixed-layer [*Dekov et al.*, 2008]. On the basis of the detailed studies by *Lackschewitz et al.* [2006] on the phyllosilicates from the Grimsey vents we suggest it is more precise to term them highly disordered talc (i.e., kerolite) instead of talc. The smectite interstratifying with kerolite in the Grimsey vent field sediments is trioctahedral, but we have not obtained enough data to conclude whether it is stevensite or saponite [*Dekov et al.*, 2008]. *Kuhn et al.* [2003] have not presented any data on this subject either and from a nomenclature point of view it is correct to name their occurrence rather kerolite-smectite using the broader term than kerolite-stevensite, which is more specific and needs particular proofs.

[40] SEM-EDS studies of Grimsey chimney samples revealed that spongy talc-like material grows on top of euhedral fibrous anhydrite crystals [*Kuhn et al.*, 2003]. The features of the studied kerolite lumps (prismatic casts in their center, concentric growth) suggest that kerolite is a primary precipitate in the hydrothermal chimneys rather

than an alteration product in the sediments. The very high formation temperatures (302–336°C; Table 2) support this suggestion. Kerolite probably precipitated after and on anhydrite crystals in the chimneys. It accumulated in the hydrothermal mounds upon the collapse of chimneys and dissolution of anhydrite (unstable at ambient temperature) leaving highly porous kerolitic beds (composed of hollow kerolite lumps with prismatic cavities), which built up the aquifer underlying the hydrothermal field. The perfectly rounded kerolite grains in the sediment indicate abrasion of kerolite lumps during mass flow transport. Core 459 SL, which contains kerolite-rich layers is located in a small valley (not visible at the scale of the map; Figure 1B) running W–E that cuts the general N–S striking slope dipping to the east. It is quite possible that frequent earthquakes [*Rögnvaldsson et al.*, 1998; *Riedel et al.*, 2001] trigger mass-gravity flows, which discharge down the slope from the proximal (<50 m) hydrothermal mounds of the Grimsey northern hill (Figure 1B). These turbidity flows have therefore dispersed the chimney rubble and scattered the kerolite lumps in the proximate sediments.

[41] The formation temperatures of kerolite (302–336°C) are similar to those previously reported for kerolite-smectite (incorrectly determined as saponite [*Lackschewitz et al.*, 2006]) from the same vent field [*Dekov et al.*, 2008]. These temperatures of kerolite precipitation have been found unreasonably high and puzzling [*Dekov et al.*, 2008] since they cannot exceed the theoretical seafloor boiling T = 250°C for the Grimsey vent field [*Hannington et al.*, 2001]. *Dekov et al.* [2008] comment on three processes that could have operated in the Grimsey Graben to produce negative $\delta^{18}O$ fluids (−4‰) required for the calculated high temperatures of formation: (1) diagenesis of sediments; (2) seawater reaction with peridotite during serpentinization; and (3) mixing of isotopically light meteoric waters with circulating seawater. All these hypotheses are somewhat speculative and need to be proven.

5.5. Chemical Fluxes During Hydrothermal Alteration

[42] The composition of altered and unaltered sediments was used to assess chemical fluxes during the hydrothermal alteration (Table 3). The chemical variations among unaltered sediments are negligible and probably a function of the relative proportions of volcanic glass, feldspars, and quartz. Two of the three mineralogically distinguishable types of alteration (smectite and kaolinite) and kerolite-rich sediments show geochemical variations, which can be correlated with differences in the processes that form the different alteration types (Table 3; Figure 9). Manganese, Rb and Sr depletion, relative to unaltered sediment, is common to the alteration processes and for the kerolitic sediments (Figures 9A, 9B, 9C, and 9F). The enrichment of Mn and Rb in the Grimsey hydrothermal fluids relative to the bottom seawater [*Lackschewitz et al.*, 2006], and Mn and Sr enrichment in the altered sediment pore fluids relative to the background sediment pore fluids (Table 4) suggests that leaching and removal of these elements away from the altered sediment causes their depletion in Mn, Rb and Sr. The alkali elements show different behavior during the sediment alteration. While Li is generally enriched and Rb is depleted in altered sediments, Cs frequently behaves conservatively during alteration (Figure 9B), although it is enriched in the hydrothermal fluids [*Lackschewitz et al.*, 2006]. The clear trend of down core increase of Li content in the altered sediment pore fluids (Table 4) testifies to hydrothermal Li input from beneath and its uptake by the sediment during alteration. Cesium depletion in the kerolitic and some kaolinitic sediments might be due either to dilution by Cs-poor minerals (kerolite, sulphates, sulfides) or to Cs removal. The Grimsey hydrothermal fluid plots exactly at the Rb/Cs regression line of the Grimsey altered sediments (Figure 9B) suggesting the sediment might have inherited the Rb/Cs ratio of the reworking fluid. Rb/Cs regression line between unaltered sediment and hydrothermal fluid (not in Figure 9B) suggests that the kerolite, 1 smectite and 2 kaolinite samples (all with low Rb/Cs ratio) might have precipitated from (in equilibrium with) hydrothermal fluid reworking background sediment. While this is certain for kerolite we suppose the smectite and kaolinite (all three samples from the lowest core sections) are result of a prolonged sediment alteration during which they have inherited the Rb/Cs ratio of the reworking hydrothermal fluid. The strong correlation between Ti, Zr, Hf, Sc, Cr, Nb and Sn (Figures 9D and 9E; Table 3) is consistent with the conservative behavior of these elements. The enrichment of these elements in the smectitic and the kaolinitic sediments and their depletion in the kerolitic sediments (Figures 9D and 9E) is not caused by their mobility, but by passive enrichment (1) and depletion (2), respectively: (1) leaching and removal of mobile elements (as the alkali and alkaline-earth elements) and residual enrichment of immobile elements; (2) dilution by precipitation of sulfates, sulfides and kerolite (with very low immobile element concentrations). A second feature common to all the altered sediments is the enrichment of U (Figure 9A) and a series of elements which behave similarly: Mo, Ba, Sb, Pb, As, Bi, Ag, Tl and Ga (Table 3). The concentrations of these elements in the altered sediment pore fluids are lower than those in the background sediment pore fluids (Table 4), which implies for uptake of these elements by the sediment during hydrothermal alteration. This accounts for the observed enrichment of the altered sediment. Enrichment of Pb (which is enriched in the hydrothermal fluids [*Lackschewitz et al.*, 2006]) could be caused by the precipitation of Pb sulfides. Base metals (Cu, Zn, Co) exhibit a similar behavior in the altered sediments. Kaolinitic sediments and part of the smectitic sediments are enriched in base metals (Figure 9F). Those samples which have base-metal concentrations below or similar to those of the background sediment are either enriched in sulfates or are surface sediments which are least altered and with low sulfide contents. This suggests that the base-metal content of the altered sediments is controlled mainly by dilution and/or enrichment produced by the precipitation of base-metal poor (sulfates) and/or base-metal rich (sulfides) phases, respectively.

[43] The alteration processes have a limited effect on the concentrations and distribution of the REE (Table 3, Figure 8). Sediments subjected to smectite alteration are slightly enriched in REE relative to the background sediment, but retain the features of the unaltered sediment: LREE-enriched relative to HREE, no Ce and Eu anomalies (Figure 8B, Table 3). The observed REE enrichment does not seem to have been the result of hydrothermal input since the Grimsey hydrothermal fluids have very low REE con-

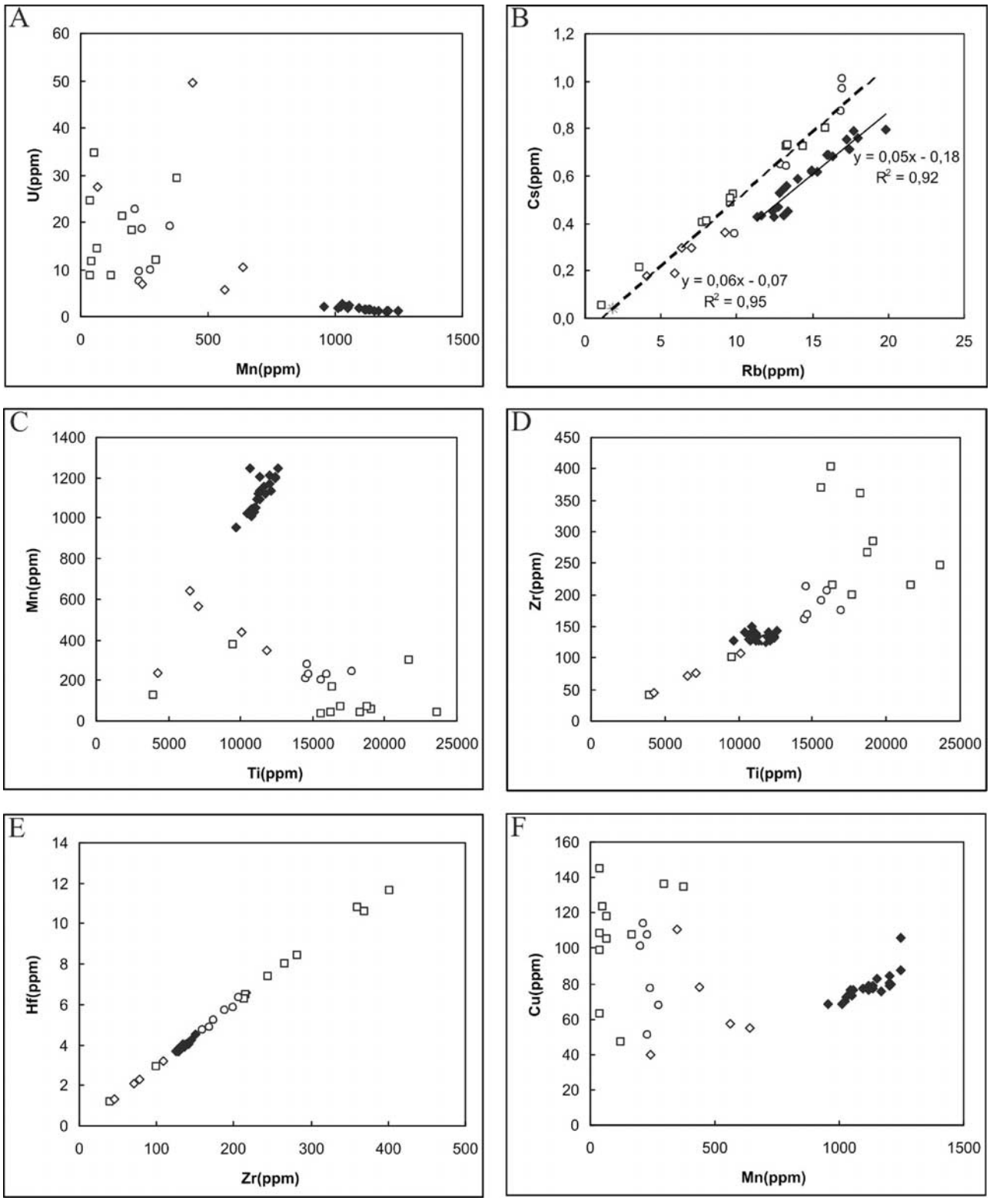

Figure 9. Plots of interelemental correlations. Closed diamonds, unaltered sediment; open circles, altered smectitic sediments; open squares, altered kaolinitic sediments; open diamonds, kerolitic sediments; star, Grimsey hydrothermal fluid [*Lackschewitz et al.*, 2006].

centrations (ΣREE = 1.8 μM/l [*Lackschewitz et al.*, 2006]). The hydrothermal leaching and removal of mobile elements such as Si, alkalis and alkaline-earths might have caused the slight REE enrichment. Pure smectite separates show enrichment in light-REE and depletion in heavy-REE relative to the background sediment and a weak negative Eu anomaly (Figure 8D). REE distribution patterns of the clay fraction composed of smectite and chlorite are smooth, with

no anomalies and are similar to those of the unaltered sediment (Figures 8C and 8D). REE patterns of the kaolinite samples (Figure 8C) are relatively smooth and show REE depletion in the lower core sections, REE enrichment in the middle core sections and REE levels of the surface sediments equal to those of the background sediment. There are 3 possible explanations of this observation: (1) leaching of the REE from the lower sediment horizons and their reprecipitation in the middle horizons; (2) passive depletion-enrichment of the REE via precipitation of sulfates (lower horizons)– leaching of mobile elements (Si, K, Na, Ca, etc.) (middle horizons); (3) enrichment/depletion is the signature of two processes: smectite and kaolinite formation. The lower sections contain kaolinite, which is depleted in the REE. The middle horizons contain smectite, which is enriched in REE, or kaolinite-smectite. Since smectite formed first, these horizons were enriched in REE. The process of smectite kaolinization would tend to reverse the REE signature but it did not progress sufficiently, as it did in the lower sections. None of the previous explanations deals with the REE signature in the surface horizons. However, these sediments show the least alteration and it is reasonable to suggest that they preserve the original REE pattern. Penetrating down bottom seawater and upwelling vent fluids at Grimsey have very low REE content ($\Sigma REE_{seawater} < 0.1$ μM, $\Sigma REE_{vent\ fluid} = 1.8$ μM [*Lackschewitz et al.*, 2006]). They hardly play a substantial role in the direct REE input to kaolinite or smectite and their function to the net REE loss/gain confines to REE redistribution in the sediment. REE distribution patterns of kerolite (Figure 8D) give 2 important clues: (1) the extremely low REE contents and strong positive Eu anomalies indicate the kerolite formed from high-temperature hydrothermal fluids, i.e., confirmed the suggestion that it formed in the hydrothermal vents; (2) the low REE content of the kerolitic sediments (Figure 8B) is due to the dilution effect of kerolite, which has low REE concentrations.

6. Conclusions

[44] Our study of the hydrothermal alteration of sediments at the Grimsey vent field has revealed:

[45] 1. The background sediments of the Grimsey Graben can be interpreted as composed of a mixture of rhyolitic and basaltic volcaniclastic material (40:60) originating from the north Icelandic volcanoes Krafla and Theistareykir, respectively.

[46] 2. These sediments are subjected to hydrothermal alteration of 3 different types, which produces smectite, kaolinite and chlorite.

[47] 3. The most common type of alteration is the smectite-type. The dominant smectite in the deepest sediments is beidellite, which decreases up core, where magnesian di-octahedral smectite (montmorillonite) and an intimate mixture of di- and tri-octahedral smectite prevail. This gradual vertical change from Al- to Mg-smectite upward suggests an increase in the Mg supply toward the seafloor. The smectite alteration is a result of sediment interaction with the ascending Si-rich hydrothermal fluids mixing with descending Mg-rich seawater. Hydrothermal leaching of primary Mg-aluminosilicates from the deeper sediments supplies additional Mg to the upper sediments.

[48] 4. There is a vertical sequence, from bottom to top, of kaolinite → mixed-layer kaolinite-smectite → smectite, which suggests the hydrothermal transformation of initially formed smectite to kaolinite through kaolinite-smectite in an environment evolving from slightly basic to slightly acidic and/or from Mg-rich to Mg-poor.

[49] 5. Ferrous chlorite (chamosite) appears as an alteration mineral replacing the detrital Mg-chlorite in veins, as Fe is made available from detrital Fe mineral dissolution.

[50] 6. Sediment alteration occurs at temperatures 95–160°C (smectite at T = 95–116°C; kaolinite at T = 150–160°C), which is consistent with measured sediment (~100°C) and vent fluid (~250°C) temperatures.

[51] 7. Kerolite precipitated at high temperatures (302–336°C) after and on anhydrite in the chimneys. It then accumulated in the hydrothermal mounds after the chimney collapse and the dissolution of anhydrite, thereby forming highly permeable aquifer layers underlying the vent field. Finally, it was scattered in the proximal sediments through turbidity flows.

[52] 8. The altered sediments have been depleted in Mn, Rb and Sr, and enriched in U, Mo, Pb, Ba, As, Bi, Sb, Ag, Tl and Ga relative to unaltered background sediment due to leaching and precipitation, respectively. They also experienced depletion and enrichment in elements with conservative behavior like Ti, Zr, Hf, Sc, Cr, Nb and Sn during the hydrothermal processes. This is a passive (precipitation or/and leaching of other phases) rather than active (due to their mobility) process. The base-metal content of the altered sediments is controlled mainly by dilution and (or) enrichment caused by precipitation of base-metal-poor and (or) base-metal-rich mineral phases (sulfates and (or) sulfides).

[53] 9. The pore fluids of altered sediment have Mg, Fe, Mn, Li and Sr concentrations higher than those of the background sediment pore fluids. The vertical distributions of these elements do not show any trend with depth in the background sediment pore fluids, while a Fe, Mn and Li content increase, and Mg and Sr decrease is observed with depth in the altered sediment pore fluids. The concentrations of U, Mo, Ba and Sb in the altered sediment pore fluids are lower than those in the background sediment pore fluids. This enrichment or depletion of the pore fluids of some elements during the hydrothermal reworking of the sediment is a result of both hydrothermal dissolution of primary minerals and hydrothermal input, or due to uptake of these elements by the sediment, respectively.

[54] **Acknowledgments.** The Alexander von Humboldt post-doctoral grant to V. M. Dekov is gratefully acknowledged. This work was funded by Deutsche Forschungsgemeinschaft through Grant SCHO 752/5-1. The International Atomic Energy Agency is grateful for the support provided to its Marine Environment Laboratories by the Government of the Principality of Monaco. We wish to thank T. Kuhn and K. Lackschewitz (both from GEOMAR, Germany) for helpful discussions, and Michael Bizimis and two anonymous reviewers for their critical remarks, which substantially improved the quality of this work.

References

Borthwick, J., and R. S. Harmon (1982), A note regarding ClF_3 as an alternative to BrF_3 for oxygen isotope analysis, *Geochim. Cosmochim. Acta*, *46*, 1665–1668.

Brindley, G. W., and G. Brown (Eds.) (1980), Crystal structures of clay minerals and their x-ray identification, *Mineral. Soc. Monogr. 5, London*, p. 495.

Buatier, M. D., G. L. Früh-Green, and A. M. Karpoff (1995), Mechanisms of Mg-phyllosilicate formation in a hydrothermal system at a sedimented ridge (Middle Valley, Juan de Fuca), *Contrib. Mineral. Petrol.*, *122*, 134–151.

Clayton, R. N., and T. K. Mayeda (1963), The use of bromine pentafluoride in the extraction of oxygen in oxides and silicates for isotopic analysis, *Geochim. Cosmochim. Acta*, *27*, 43–52.

Dekov, V. M., J. Scholten, R. Botz, C.-D. Garbe-Schönberg, M. Thiry, P. Stoffers, and M. Schmidt (2005), Occurrence of kaolinite and mixed-layer kaolinite/smectite in hydrothermal sediments of Grimsey Graben, Tjörnes Fracture Zone (north of Iceland), *Mar. Geol.*, *215*, 159–170.

Dekov, V. M., J. Cuadros, W. C. Shanks, and R. A. Koski (2008), Deposition of talc-kerolite-smectite-smectite at seafloor hydrothermal vent fields: Evidence from mineralogical, geochemical and oxygen isotope studies, *Chem. Geol.*, *247*, 171–194.

de Oliveira, C. G., and R. V. Santos (2003), Isotopic domains controlled by transtensional and transpressional sectors in the auriferous Diadema shear belt, northern Brazil, *J. South Am. Earth Sci.*, *16*, 513–522.

Devey, C. W., C.-D. Garbe-Schönberg, P. Stoffers, C. Chauvel, and D. F. Mertz (1994), Geochemical effects of dynamic melting beneath ridges: Reconciling major and trace element variations in Kolbeinsey (and global) mid-ocean ridge basalt, *J. Geophys. Res.*, *99*, 9077–9095.

Edmond, J. M., C. Measures, R. E. McDuff, L. H. Chan, R. Collier, B. Grant, L. I. Gordon, and J. B. Corliss (1979), Ridge crest hydrothermal activity and the balances of the major and minor elements in the ocean: The Galapagos data, *Earth Planet. Sci. Lett.*, *46*, 1–18.

Garbe-Schönberg, D. (1993), Simultaneous determination of 37 trace elements in 28 international rock standards by ICP/MS, *Geostand. Newsl.*, *17*, 81–97.

Goodfellow, W. D., and B. Blaise (1988), Sulfide formation and hydrothermal alteration of hemipelagic sediment in Middle Valley, northern Juan de Fuca Ridge, *Can. Mineral.*, *26*, 675–696.

Hannington, M., P. Herzig, P. Stoffers, J. Scholten, R. Botz, D. Garbe-Schönberg, I. R. Jonasson, W. Roest, and Shipboard Scientific Party (2001), First observations of high-temperature submarine hydrothermal vents and massive anhydrite deposits off the north coast of Iceland, *Mar. Geol.*, *177*, 199–220.

Hemond, C., N. T. Arndt, U. Lichtenstein, A. W. Hofmann, N. Oskarsson, and S. Steinthorsson (1993), The heterogeneous Iceland plume: Nd-Sr-O isotopes and trace element constraints, *J. Geophys. Res.*, *98*, 15,833–15,850.

Howard, K. J., and M. R. Fisk (1988), Hydrothermal alumina-rich clays and boehmite on the Gorda Ridge, *Geochim. Cosmochim. Acta*, *52*, 2269–2279.

Huertas, F. J., S. Fiore, F. Huertas, and J. Linares (1999), Experimental study of the hydrothermal formation of kaolinite, *Chem. Geol.*, *156*, 171–190.

Komninou, A., and D. A. Sverjensky (1995), Pre-ore hydrothermal alteration in an unconformity-type uranium deposit, *Contrib. Mineral. Petrol.*, *121*, 99–114.

Koski, R. A., P. F. Lonsdale, W. C. Shanks, M. E. Berndt, and S. S. Howe (1985), Mineralogy and geochemistry of a sediment-hosted hydrothermal sulfide deposit from the Southern Trough of Guaymas Basin, Gulf of California, *J. Geophys. Res.*, *90*, 6695–6707.

Kuhn, T., P. M. Herzig, M. D. Hannington, D. Garbe-Schönberg, and P. Stoffers (2003), Origin of fluids and anhydrite precipitation in the sediment-hosted Grimsey hydrothermal field north of Iceland, *Chem. Geol.*, *202*, 5–21.

Kulla, J. P., and T. F. Anderson (1978), Experimental oxygen isotope fractionation between kaolinite and water, in *Short Papers of the 4th Inter. Conf., Geochron., Cosmochron., Isotope Geol., 1978, U. S. Geol. Surv., Open File Rep. No. 78-70*, edited by R. E. Zartman, pp. 234–235.

Lackschewitz, K. S., A. Singer, R. Botz, D. Garbe-Schönberg, P. Stoffers, and K. Horz (2000), Formation and transformation of clay minerals in the hydrothermal deposits of Middle Valley, Juan de Fuca Ridge, ODP Leg 169, *Econ. Geol.*, *95*, 361–389.

Lackschewitz, K. S., R. Botz, D. Garbe-Schönberg, J. Scholten, and P. Stoffers (2006), Mineralogy and geochemistry of clay samples from active hydrothermal vents off the north coast of Iceland, *Mar. Geol.*, *225*, 177–190.

Lonsdale, P. F., J. L. Bischoff, V. M. Burns, M. Kastner, and R. E. Sweeney (1980), A high-temperature hydrothermal deposit on the seabed at a Gulf of California spreading center, *Earth Planet. Sci. Lett.*, *49*, 8–20.

Matsuhisa, Y. (1974), $^{18}O/^{16}O$ ratios for NBS-28 and some silicate reference samples, *Geochem. J.*, *8*, 103–107.

Mehra, O. P., and M. L. Jackson (1960), Iron oxide removal from soils and clays by dithionite-citrate system buffered with sodium bicarbonate, *Clays Clay Miner.*, *7*, 317–327.

Moore, D. M., and C. R. Reynolds Jr. (1989), *X-ray Diffraction and the Indentification and Analysis of Clay Minerals*, p. 332, Oxford Univ. Press, New York.

Mottl, M. J. (1983), Metabasalts, axial hot springs, and the structure of hydrothermal systems at mid-ocean ridges, *Geol. Soc. Am. Bull.*, *94*, 161–180.

Mottl, M. J., and H. D. Holland (1978), Chemical exchange during hydrothermal alteration of basalt by seawater. I: Experimental results for major and minor components of seawater, *Geochim. Cosmochim. Acta*, *42*, 1103–1115.

Percival, J. B., and D. E. Ames (1993), Clay mineralogy of active hydrothermal chimneys and an associated mound, Middle Valley, northern Juan de Fuca Ridge, *Can. Mineral.*, *31*, 957–971.

Riedel, C., M. Schmidt, R. Botz, and F. Theilen (2001), The Grimsey hydrothermal field offshore North Iceland: Crustal structure, faulting and related gas venting, *Earth Planet. Sci. Lett.*, *193*, 409–421.

Rögnvaldsson, S., A. Gudmundsson, and R. Slunga (1998), Seismotectonic analysis of the Tjörnes Fracture Zone, an active transform fault in north Iceland, *J. Geophys. Res.*, *103*, 30,117–30,129.

Saccocia, P. J., and K. M. Gillis (1995), Hydrothermal upflow zones in the oceanic crust, *Earth Planet. Sci. Lett.*, *136*, 1–16.

Savin, S. M., and M. Lee (1988), Isotopic studies of phyllosilicates, in *Hydrous Phyllosilcates (Excusive of Micas)*, edited by S. W. Bailey, *Rev. Mineral.*, *19*, 189–223, Mineralogical Society of America, Washington, D. C.

Siffert, B. (1962), Quelques reactions de la silice en solution: La formation des argiles, *Mem. Serv. Carte Geol. Alsace-Lorraine*, *21*, 1–86.

Slater, L., M. Jull, D. McKenzie, and K. Gronvöld (1998), Deglaciation effects on mantle melting under Iceland: Results from the northern volcanic zone, *Earth Planet. Sci. Lett.*, *164*, 151–164.

Stracke, A., A. Zindler, V. J. M. Salters, D. McKenzie, J. Blichert-Toft, F. Albarède, and K. Grönvold (2003), Theistareykir revisited, *Geochem. Geophys. Geosyst.*, *4*(2), 8507, doi:10.1029/2001GC000201.

Sun, S.-S., and W. F. McDonough (1989), Chemical and isotopic systematics of oceanic basalts: Implications for mantle composition and processes, in *Magmatism in the Ocean Basins*, edited by A. D. Saunders and M. J. Norry, *Geol. Soc. London, Spec. Publ.*, *42*, 313–345, Blackwell Scientific Publications, Oxford, UK.

Von Damm, K. L., J. M. Edmond, B. Grant, C. I. Measures, B. Walden, and R. F. Weiss (1985a), Chemistry of submarine hydrothermal solutions at 21°N, East Pacific Rise, *Geochim. Cosmochim. Acta*, *49*, 2197–2220.

Von Damm, K. L., J. M. Edmond, C. I. Measures, and B. Grant (1985b), Chemistry of submarine hydrothermal solutions at Guaymas Basin, Gulf of California, *Geochim. Cosmochim. Acta*, *49*, 2221–2237.

Von Damm, K. L., C. M. Parker, R. A. Zierenberg, M. D. Lilley, E. J. Olson, D. A. Clague, and J. S. McClain (2005), The Escanaba Trough, Gorda Ridge hydrothermal system: Temporal stability and subseafloor complexity, *Geochim. Cosmochim. Acta*, *69*, 4971–4984.

Zierenberg, R. A., and W. C. Shanks III (1994), Sediment alteration associated with massive sulfide formation in Escanaba Trough, Gorda Ridge: The importance of seawater mixing and magnesium metasomatism, in *Geologic, Hydrothermal, and Biologic Studies at Escanaba Trough, Gorda Ridge, Offshore Northern California*, edited by J. L. Morton, R. A. Zierenberg, and C. A. Reiss, *U. S. Geol. Surv. Bull.*, *2022*, 257–277.

R. Botz, C.-D. Garbe-Schönberg, and P. Stoffers, Christian-Albrechts-University Kiel, Institute of Geosciences, Department of Geology, Ludewig-Meyn-Strasse 10, D-24118 Kiel, Germany.

J. Cuadros, Department of Mineralogy, Natural History Museum, Cromwell Road, London SW7 5BD, UK.

V. Dekov, Department of Geology and Paleontology, University of Sofia, 15, Tzar Osvoboditel Boulevard, Sofia 1000, Bulgaria. (dekov@gea.uni-sofia.bg)

M. Schmidt, Leibniz-Institut für Meereswissenschaften, IFM-Geomar, East Building (8E-108), Wischhofstr. 1–3, D-24148 Kiel, Germany.

J. Scholten, International Atomic Energy Agency, Marine Environment Laboratories, 4, Quai Antoine 1er, MC-98000 Monaco, Monaco.